Mohamed Saleh *et al. Carbon Research* (2025) 4:60
https://doi.org/10.1007/s44246-025-00227-3

Carbon Research

ORIGINAL ARTICLE Open Access

Enhanced CO_2 capture using KOH-functionalized oil palm ash adsorbent: experimental and applied machine learning approach

Syamima Nasrin Mohamed Saleh[1], Fakhrony Sholahudin Rohman[2], Dinie Muhammad[3], Syafini Mohd Hussin[1], Bassim H. Hameed[4], Chew Thiam Leng[5] and Azam Taufik Mohd Din[1*]

Abstract

This work aimed to develop a cost-effective, environmentally friendly, and sustainable adsorbent for CO_2 capture using biomass waste, specifically oil palm ash (OPA), which is abundantly available as agricultural waste in Malaysia. Pristine OPA was first subjected to acid washing, followed by carbonization and chemical activation with KOH to enhance its physicochemical properties. Since machine learning (ML) can provide new insights into the design of adsorption processes and the understanding of CO_2 adsorption mechanism, this paper presents a detailed comparative analysis of experimental and ML approaches. In this study, the surface and pore characteristics of OPA-KOH(1:2) were significantly enhanced through carbonization and KOH-functionalization, achieving an optimized mesoporous structure (average pore size: 72.71 Å), with a surface area of 30.95 m^2/g. Despite having a moderate surface area, the tailored pore structure promoted efficient CO_2 diffusion, thus enabling high CO_2 adsorption capacity of 2.9 mmol/g, which was comparable or exceeds that some Acs with higher surface areas. Systematic analyses of adsorption isotherms, kinetics, and thermodynamics have confirmed that the CO_2 adsorption onto OPA-KOH(1:2) occurred exothermically and was predominantly driven by a physisorption mechanism, supported by a weak chemisorption mechanism. ML-based models employed in this study have demonstrated that the bilayered neural network (NN) model could accurately predict CO_2 adsorption onto OPA-KOH(1:2), with exceptionally high accuracy of $R^2 > 0.99$. These findings have provided valuable insights into the capture, conversion, utilization, and storage (CCUS) technology, while highlighting OPA-KOH(1:2) as an affordable and environmentally friendly adsorbent for effective CO_2 capture.

Highlights

- OPA-KOH(1:2) exhibited enhanced CO_2 capture performance with a capacity of 2.9 mmol/g.
- CO_2 adsorption onto OPA-KOH(1:2) was characterized by heterogeneous, exothermic, and physisorption-dominated mechanisms.
- The bilayered neural network machine learning model was capable of accurately predicting CO_2 adsorption behavior under different operating conditions.
- KOH-functionalized OPA has demonstrated significant potential for a sustainable carbon capture process.

*Correspondence:
Azam Taufik Mohd Din
chazam@usm.my
Full list of author information is available at the end of the article

Keywords Carbon dioxide adsorption, Oil palm ash-based adsorbent, KOH activation, Machine learning, Bilayered neural network model

Graphical Abstract

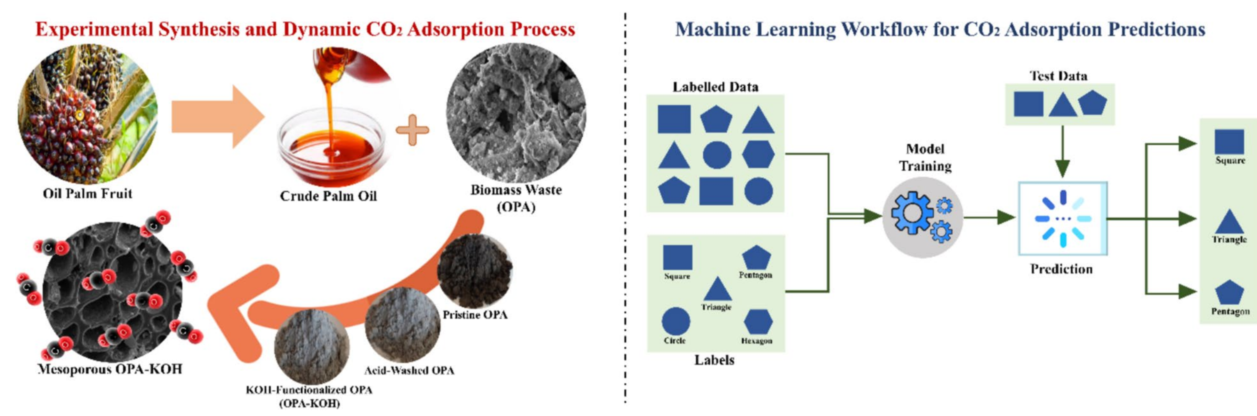

1 Introduction

Effective control and management of CO_2 emissions is urgently needed to counter the rapidly increasing global greenhouse gas emissions, driven by advances in science, technology, and rapid economic development (Huang et al. 2024). According to the International Energy Agency (IEA), CO_2 emissions have increased by more than 50% over the past century, reaching 36.8 Gt in 2022 (Chen 2023), primarily from combustion and industrial activities such as cement, iron, steel, and petrochemical industries. In response, carbon capture, utilization, and storage (CCUS) technologies have gained attention as promising mitigation strategies (Bai et al. 2023b; MIDA 2023a, b; Ishak et al. 2024; Naseer et al. 2022). Among these available approaches, adsorption-based CO_2 capture has been widely investigated due to its high selectivity, reusability, energy efficiency, and cost-effectiveness (Das et al. 2023; Rafique et al. 2024).

Various solid adsorbents, such as zeolites, silicon-based materials (Policicchio et al. 2022), metal–organic frameworks (MOFs) (Ali et al. 2023), porous polymers (Bai et al. 2023a; Sun et al. 2015), zeolites (Chatterjee et al. 2021; Tsiotsias et al. 2023), and activated carbon (AC) (Bai et al. 2024; Ke et al. 2022; Siriwardane et al. 2001), have been developed to enhance CO_2 capture efficiency. Among them, AC materials have demonstrated superior chemical, mechanical, and thermal stability, along with excellent moisture resistance and lower energy requirements for regeneration (González and Manyà 2020). The properties of AC, such as surface area, porosity, and CO_2 uptake capacity, are significantly influenced by the choice of activation agent. Various chemical activation agents have been employed, including phosphoric acid (H_3PO_4) (Lu et al. 2022), sodium hydroxide (NaOH) (Guo et al. 2020), zinc chloride ($ZnCl_2$) (Lu et al. 2022; Sarwar et al. 2021), and potassium hydroxide (KOH) (Lu et al. 2022), with each imparting different structural characteristics to the final adsorbent. A previous study has shown that H_3PO_4 activation at relatively low temperatures of 450 ^{0}C could produce ACs with surface areas exceeding 359 m^2/g (Fierro et al. 2010). Similarly, $ZnCl_2$ activation has been reported to yield highly microporous structures with enhanced CO_2 adsorption selectivity (Sarwar et al. 2021). However, KOH activation is widely recognized for producing well-developed mesoporous and microporous structures with optimized adsorption kinetics. While KOH-activated materials may exhibit moderate surface areas, they often achieve higher CO_2 uptake efficiencies due to improved pore connectivity and tunable functional groups (Alabadi et al. 2015; Pang et al. 2021). In this study, OPA was activated using KOH due to the ability of KOH to create a balanced meso-microporous network, which is crucial for enhancing CO_2 diffusion and adsorption efficiency.

Chemical activation methods, particularly KOH activation, have been extensively applied to enhance the properties of AC materials by increasing their surface area, microporosity, and adsorption capacity (Abuelnoor et al. 2021; Siriwardane et al. 2001). In addition to improving adsorbent efficiency, the sustainability aspect of AC adsorbents in carbon capture technologies has gained increasing attention. The agricultural sector accounts for approximately 21% of total greenhouse gas emissions, producing 998 tons of agricultural waste annually. The transformation of agricultural waste into AC adsorbents presents an eco-friendly and cost-effective solution that could simultaneously mitigate environmental pollution and enhance carbon capture capabilities (Karić et al. 2022). Several agricultural wastes (Azmi et al. 2024), such as spent coffee grounds (Czerwinska et al. 2024), palm oil mill fly ash (Kongnoo et al. 2017), sugar bagasse (Guo et al. 2020), and rice husks (Wang et al. 2022), have been successfully converted into AC for CO_2 adsorption. As one of the world's leading palm oil producers, Malaysia generates vast amounts of palm-oil related waste, including oil palm ash (OPA). OPA, a byproduct of the combustion of palm kernel shells and fibers in palm oil mills, is often discarded in landfills, causing environmental hazards and waste disposal challenges. The repurposing of OPA into KOH-functionalized AC presents a sustainable, low-cost, and effective solution for CO_2 capture (Aisheh 2023). Despite these advances, most CO_2 adsorption studies have relied heavily on empirical measurements and theoretical models, which could often oversimplify complex adsorption behaviors. Traditional adsorption models, such as the Langmuir (Langmuir 1918) and Freundlich (Freundlich 1906) isotherms, could provide useful approximations but have failed to capture the full complexity of adsorption mechanisms in heterogeneous porous materials. Additionally, experimental studies require substantial time and costs, thus limiting large-scale implementation. To overcome these challenges, machine learning (ML) approaches have recently gained interest in predictive modeling for CO_2 capture.

Although ML techniques have been successfully applied in various scientific fields, their application in CO_2 adsorption modeling remains limited. Most previous studies have independently explored either adsorption performance or predictive modeling, with minimal integration of experimental results into ML-based frameworks. There is still a lack of research that systematically correlates experimental CO_2 adsorption conditions with predictive analytics to optimize CO_2 capture performance. This study aimed to bridge these gaps by integrating experimental processing with ML-based predictive modeling to evaluate and optimize CO_2 adsorption performance using KOH-functionalized OPA-derived AC. The experimental approach was applied to systematically investigates the effects of process parameters (i.e., OPA-to-KOH ratio, flow rate, temperature, and initial CO_2 concentration) on CO_2 capture performance. The resulting dataset was then used to train and validate ML models, namely decision tree (DT), support vector machine (SVM), and artificial neural networks (ANN). Unlike conventional empirical models, ML could provide a highly accurate, adaptable, and scalable solution for predicting CO_2 capture performance under different process conditions. By employing DT, SVM, and ANN, this study aimed to demonstrate how ML could be used to reduce experimental workload, and improve industrial applicability. Hence, this dual approach could provide a scalable methodology for real-world applications, making a valuable contribution to the field of carbon capture and environmental sustainability.

2 Materials and methods

2.1 Biomass source, chemicals and gases

Oil palm ash (OPA), sourced from the United Oil Palm Mill in Pulau Pinang, Malaysia, was selected as the adsorbent material for this study. Other chemicals, including hydrochloric acid (HCl, 37%) and potassium hydroxide (KOH, ≥98%), were acquired from Merck Sdn. Bhd., Selangor, Malaysia. Carbon dioxide gas (CO_2, 99.9%) and nitrogen gas (N_2, 99.9%) were procured from Wellgas (M) Sdn. Bhd.

2.2 Synthesis of KOH-functionalized OPA

Pristine OPA was washed with 1.0 M HCl to remove excess ash and contaminants. The standard method used in this work for preparing the adsorbent material was modified based on the method outlined by Zainudin and co-workers (Zainudin et al. 2005). Next, the OPA was rinsed with warm distilled water until its pH reached 7. It was then filtered and dried overnight at 105 °C to remove moisture. A specific amount of KOH was added to distilled water and stirred until it was completely dissolved. Then, a specific amount of OPA was added to the KOH solution and stirred for 5 h at an intermediate stirring rate. The resulting mixture was heated for 8 h with gentle stirring at 90 °C in a reflux column. The heated mixture was then placed in a water bath shaker at 50 °C and 150 rpm to soak the KOH-impregnated OPA for 1 h. Next, the OPA was dried overnight at 60 °C before being carbonized at 700 °C in a horizontal tubular furnace for 1 h at a heating rate of 10 °C/min under nitrogen flow at 150 mL/min. This temperature was chosen because it was widely reported in the literature as being able to optimize the pore development and enhance the surface area of biomass-derived activated carbon materials. At this temperature, the removal of volatile organic components and the formation of an enhanced porous structure would be facilitated without significant structural degradation. Lower carbonization temperatures (< 600 °C) have been shown to result in incomplete carbonization and lower porosity, while higher temperatures (> 800 °C) could lead to pore collapse due to excessive carbon burn-off (Gayathiri et al. 2022; Quan et al. 2021). The adsorbent material was denoted as OPA-KOH(x), with x representing the OPA-to-KOH ratio.

2.3 Characterization of adsorbent materials

A nitrogen physisorption analysis was performed using a Micromeritics ASAP 2020 to investigate the surface and pore characteristics of the pristine OPA, acid-washed OPA, and OPA-KOH(1:2) adsorbents. The samples were degassed ($P < 10^{-1}$ Pa) for 6 h at 300 °C to remove any impurities. The Brunauer–Emmett–Teller (BET) method was used to determine the specific surface areas, while the pore size distributions of the synthesized adsorbents were analyzed using the Barrett-Joyner-Halenda (BJH) model. To compare and examine the changes in the appearance of the surface morphological structure of the adsorbents, the Field Emission Scanning Electron Microscopy (FESEM) analysis was conducted. FESEM micrographs were taken using a Quanta FEG 450 FESEM. This instrument was operated at an accelerating voltage of 1–30 kV with a spatial resolution of 1.2 nm at 30 kV in high vacuum mode. Fourier Transform Infrared (FTIR) spectra were recorded using the potassium bromide (KBr) pellet technique by employing a Perkin-Elmer 2000 Spectrometer at room temperature. FTIR analysis was performed to determine the specific chemical bonds within OPA and OPA-KOH(1:2) samples. To conduct this procedure, 0.9 mg of each sample was thoroughly mixed with 63 mg of KBr, grounded using an agate mortar, and pressed into a pellet. The IR spectra obtained from the analysis were recorded in the wavelength range of 4000 to 400 cm^{-1}, with a detection limit of 0.1 absorbance unit.

2.4 Dynamic adsorption process analysis

Dynamic adsorption experiments were conducted using a fixed-bed column with a radius of 0.55 cm and a height of 14 cm to examine the isotherms, kinetics, and thermodynamics of CO_2 uptake using OPA-KOH(x) adsorbents. To start, 0.5 g of OPA-KOH(x) sample was loaded into the fixed-bed column. The column was then heated to 110 °C and kept at this temperature for 1 h, while a continuous flow of nitrogen (N_2, 90 mL/min) passed through to remove excess moisture. After the column was allowed to cool down to 30 °C, the desired gas mixture (1:9 vol.% of CO_2-to-N_2) was introduced at the specified flow rate. CO_2 concentration was continuously monitored using a Quantek 906 CO_2 analyzer (detection limit: 20 ppm, accuracy: ± of full scale), which was connected to a computer via a HOBO data logger, with all data recorded using the HOBOware Pro software. The adsorption process was stopped once the CO_2 concentration reached equilibrium. The effects of various parameters, namely OPA-to-KOH ratio (1:0.5, 1:1, 1:2, and 1:3), flow rate (30–60 mL/min), temperature (30–60 °C), and initial CO_2 concentration (7%–15%), on the adsorption process were investigated. To ensure the repeatability and reliability of the results, each adsorption test was conducted in triplicate for each parameter.

The following Eq. (1) was used to calculate the adsorption capacities of the adsorbent materials:

$$q = \frac{C_0 F_0}{m} \int_0^t \left(1 - \frac{C}{C_0}\right) dt \tag{1}$$

where q refers to CO_2 adsorption capacity (mg/g); C_0 refers to the concentration of CO_2 at the inlet ($vol.\%$); F_0 refers to the volumetric flow rate of CO_2 (mL/min); m refers to the mass of the adsorbent material (g); and C_t refers to the concentration of CO_2 at the outlet ($vol.\%$).

2.5 Development of theoretical models

2.5.1 Adsorption isotherms

This study has examined CO_2 capture using OPA-KOH adsorbents at different ratios (1:0.5, 1:1, 1:2, and 1:3) across a temperature range of 30–60 °C, while applying the Langmuir and Freundlich isotherm models. Equations (2) and (4) represent the general equations for Langmuir and Freundlich isotherm models, respectively. Equation (2), representing the Langmuir isotherm model, illustrates typical monolayer adsorption on uniform sites (Langmuir 1918):

$$q_e = \frac{q_{max} k_L P_{CO_2}}{1 + k_L P_{CO_2}} \tag{2}$$

where q_e refers to the equilibrium amount of CO_2 adsorbed per gram of adsorbent (mmol/g); q_{max} refers to the maximum CO_2 uptake onto the OPA-KOH(1:2), which indicates a complete monolayer coverage ($mmol/g$); P_{CO_2} refers to the partial pressure of CO_2 (bar); and k_L refers to the Langmuir constant or affinity constant related to the adsorption rate and capacity (bar^{-1}). Meanwhile, the dimensionless separation factor, R_L, which indicates the favourability of adsorption in Langmuir isotherm, is calculated using the following Eq. (3).

$$R_L = \frac{1}{1 + k_L C_0} \tag{3}$$

where k_L refers to the Langmuir constant (bar^{-1}); and C_0 refers to the initial concentration of CO_2.

The Freundlich isotherm model, which observes the heterogeneity that arises from the characteristics of the adsorption sites and the corresponding number of adsorbed molecules, would suggest multilayer adsorption on heterogeneous adsorbents. As the number of adsorbed molecules increases, the probability of binding, or binding capacity, decreases due to the exponential rise in energy requirements. The following Eq. (4) shows the empirical representation of the Freundlich isotherm model (Ammendola et al. 2017; Freundlich 1906):

$$q_{CO_2} = k_F P^{1/n_F} \tag{4}$$

where q_{CO_2} refers to the amount of CO_2 adsorbed per gram of OPA-KOH(1:2) (mmol/g); k_F refers to the Freundlich or temperature-dependent constant ($mmol/g.bar$); P refers to the relative pressure of CO_2 (bar); and n_F refers to the heterogeneity factor, which indicates the degree of linearity between the adsorbate solution and the adsorption process. In Eq. (4), $\frac{1}{n_F}$ indicates the intensity parameter that reflects the driving force or the surface heterogeneity. The value of n_F characterizes the type of adsorption interaction. When $n_F = 1$, the adsorption is linear, while when $n_F < 1$, the adsorption involves chemical interactions, whereas when $n_F > 1$, the adsorption involves physical interactions. An adsorption is considered favorable when $0 \leq \frac{1}{n_F} \leq 1$ and cooperative adsorption occurs when $\frac{1}{n_F} > 1$ (Fatima et al. 2023).

2.5.2 Adsorption kinetics

Pseudo-first order and pseudo-second order kinetic models were used to describe the adsorption kinetics of CO_2 on OPA-KOH(1:2) adsorbent, as represented by Eqs. (5) and (6), respectively. The pseudo-first order kinetics applies primarily to physical adsorption, as it describes the relationship between the adsorption rate and the availability of the adsorbents' active sites. Several assumptions are made to simplify this kinetic model. First, the rate of change in solute uptake with time is directly proportional to the difference between the saturation concentration and the amount of solute uptake by the solid. Second, this model is only applicable during the initial stage of the adsorption process. Equation (5) shows the pseudo-first order kinetic model:

$$q_t = q_e\left(1 - e^{-k_1 t}\right) \tag{5}$$

where q_t refers to the adsorption capacity of OPA-KOH(1:2) at time t (mg/g); q_e refers to the adsorption capacity of OPA-KOH(1:2) at equilibrium (mg/g); k_1 refers to the first-order reaction rate constant (min^{-1}); and t refers to the time (min). Equation (6) shows the pseudo-second order kinetic model:

$$q_t = \frac{k_2 {q_e}^2 t}{1 + k_2 q_e t} \tag{6}$$

where, k_2 represents the second-order reaction rate constant ($g/mg.min$).

2.5.3 Adsorption thermodynamics

CO_2 adsorption was conducted at temperatures ranging from 30–60 °C to determine the thermodynamic parameters while the optimized operational conditions were kept constant during batch adsorption experiments. The enthalpy change ($\triangle H°$), entropy change ($\triangle S°$), and Gibbs free energy change ($\triangle G°$) were calculated through thermodynamic analysis. $\triangle G°$ was computed using Eq. (7), whereby lnk_F was calculated using the Van't Hoff equation (Eq. (8)) by plotting lnk_F versus$1/T$. The slope and intercept of the Van't Hoff plot provided the values for $\triangle H°$ and $\triangle S°$, respectively (Nareswari et al. 2024).

$$\Delta G^0 = -RT\ln k_F \tag{7}$$

$$\ln k_F = -\frac{\Delta H^0}{RT} + \frac{\Delta S^0}{R} \tag{8}$$

2.6 Development of machine learning models

The consistency and performance of any ML-based model depend heavily on the quality of the dataset used for training. In this work, a comprehensive dataset of 346 experimental measurements was collected to represent CO_2 adsorption capacity (mmol/g) for various combinations of four input parameters, namely OPA-to-KOH ratio, flow rate, temperature, and initial CO_2 concentration. In this work, the ML model was developed based on the decision tree (DT), support vector machine (SVM), and artificial neural network (ANN) using the available functions in MATLAB.

2.6.1 Data pre-processing and division

In this study, the dataset, consisting of experimental CO_2 adsorption capacity results was imported into MATLAB where predictor and response variables were automatically assigned. Feature selection was performed, with all predictor variables (OPA-to-KOH ratio, flow rate, temperature, initial concentration) retained for training. Table 1 summarizes the input and output parameters, along with their respective ranges, that have been used for developing the ML models.

2.6.2 Model training

The ML function in MATLAB enabled the automated training of multiple model types, including DTs, SVMs, and NNs. Default hyperparameters were used without enabling optimization to ensure a balance between model complexity and training time. These models

Table 1 Input–output parameters and their respective ranges in the training dataset for DT, SVM and ANN models

Experimental parameter	Unit	Range	
		Minimum	Maximum
Input			
OPA-to-KOH ratio (R)		0.33	2
Flow rate (F)	mL/min	30	60
Temperature (T)	^{0}C	30	60
Initial concentration (C)	vol.%	7	15
Time (t)	min	0	50
Output			
Adsorption capacity (AC)	mmol/g	0	3

were trained using Mean Squared Error (MSE) as the loss function and evaluated based on their predictive accuracy.

2.6.3 Model validation

A fivefold cross-validation method was applied to prevent overfitting and to obtain a robust performance estimate. In this approach, the dataset was partitioned into five subsets, with the model trained on four subsets and validated on the fifth to ensure that each subset could serve as a validation set once.

2.6.4 Evaluation of ML models for CO_2 capture performance

Decision tree Decision tree (DT) is a supervised ML algorithm commonly used for classification and regression tasks. It predicts responses by recursively splitting the dataset into subsets based on feature values to form a tree-like structure. Each split is designed to maximize information gain or minimize impurity measures (e.g., Gini impurity or entropy), while ensuring optimal partitioning of the data. There are three main types of DT models, namely fine, medium, and coarse. These terms refer to different configurations of DTs, primarily based on their depth and number of splits. These configurations control the model's complexity by balancing between underfitting and overfitting (MathWorks 2024a, b, c, d).

A fine DT model has high depth and numerous splits, thus enabling detailed partitioning of the feature space. A medium DT model balances tree depth and leaf size to offer moderate complexity while a coarse DT model simplifies the decision process by limiting tree depth and the number of splits, which would result in a shallower tree. The binary DT models for different classifications were fitted in MATLAB using the *fitctree* function. The codes, as shown by Eqs. (9, 10, 11), were applied to the fine, medium, and coarse DT models, respectively (MathWorks 2024a, b, c, d):

$$model = fitctree(X,\ Y\ 'MaxNumSplits',\ largeValue) \quad (9)$$

$$model = fitctree(X, Y,' MaxNumSplits', mediumValue) \quad (10)$$

$$model = fitctree(X, Y,' MaxNumSplits', smallValue) \quad (11)$$

Support vector machine SVM is a powerful supervised ML algorithm used for classification and regression tasks. SVM regression is often classified as a nonparametric technique because it relies solely on kernel functions. It works by identifying the hyperplane that best separates data points into different classes. An optimal hyperplane is the one that maximizes the margin between the closest data points of each class, which are referred to as support vectors. The choice of kernel function determines how the SVM maps input data into a higher-dimensional space to find a suitable separating hyperplane. The terms linear SVM, quadratic SVM, and cubic SVM refer to the specific types of kernel function used, which are linear, quadratic, or cubic (MathWorks 2024a, b, c, d).

As the name suggests, a linear SVM uses a linear kernel to separate data. It works well when the dataset is linearly separable, meaning that a straight line (or hyperplane) can divide the classes in the feature space. The training dataset for the SVM model consists of a multivariate set of N observations, $\{ (x_1,y_1),\ldots,(x_N,y_N)\}$, where x_N represents the input vector. In general, the linear kernel function is as shown in Eq. (12):

$$K(xi, xj) = xi.xj \quad (12)$$

This means no transformation of data is applied, and the algorithm directly works in the original feature space. The MATLAB function *fitcsvm* can be used to train or cross-validate an SVM classifier for one-class and binary classifications (MathWorks 2024a, b, c, d). This function can be written as shown in Eq. (13):

$$model = fitcsvm(X, Y,' KernelFunction',' linear') \quad (13)$$

A quadratic SVM uses a polynomial kernel of degree 2, which enables non-linear decision boundaries to model more complex relationships between feature spaces. It is suitable when the dataset is not linearly separable but can be separated by a quadratic boundary. The polynomial kernel function of degree 2 can be expressed as shown in Eq. (14):

$$K(xi, xj) = (xi.xj + 1)2 \quad (14)$$

This maps the original feature space into a higher-dimensional space, thus enabling the capture of quadratic relationships. This function is coded as shown in Eq. (15):

$$model = fitcsvm(X, Y,' KernelFunction',' polynomial',' PolynomialOrder', 2) \tag{15}$$

A cubic SVM uses a polynomial kernel of degree 3, offering greater flexibility than a quadratic kernel by allowing more complex non-linear boundaries. It is suitable for data with higher complexity that requires a more intricate decision boundary. The polynomial kernel function of degree 3 is expressed as follows:

$$K(xi, xj) = (xi.xj + 1)3 \tag{16}$$

This maps the input dataset into an even higher-dimensional feature space, enabling the model to fit more complex data structures. This function is written as shown in Eq. (17):

$$model = fitcsym\left(X, Y,' KernelFunction', \ 'polynomial', \ 'PolynomialOrder', 3\right) \tag{17}$$

Artificial neural network A neural network (NN) is a computational model inspired by the structure and function of biological neural networks in the human brain. It is designed to recognize and model complex relationships, patterns, and solve regression effectively. At its core, a neural network consists of layers of neurons (nodes) that can process input data and propagate information forward through the network to produce an output. The architecture of NN models may include several layers, such as an input layer (*i*), hidden layers (*h*), and output layers. Figure 1 shows the structure of the ANN model used in this study.

In this work, CO_2 capture on OPA-KOH(1:2) was modeled using two types of NN models, namely the narrow NN and the bilayered NN. A narrow NN typically consists of a single hidden layer with a limited number of neurons, making it suitable for modeling simple relationships. It can be effectively implemented using the *fitnet* function in MATLAB for regression tasks. A bilayered NN, on the other hand, differs from the simple narrow NN and is characterized by two hidden layers, enabling it to capture more complex patterns in the dataset. This type of network can also be implemented in MATLAB, using the same function but with a different architectural setup. Models with multilayer structures are more effective at learning representations and extracting features.

2.6.5 Model configuration

The default settings of the ML function in MATLAB have ensured that the developed models could be trained efficiently while maintaining optimal performance. The default hyperparameter configurations for each model type were as follows:

a) *Decision Tree*
   Fine tree: 100 maximum splits, minimum leaf size of 4, split criterion: MSE.
   Medium tree: 20 maximum splits, minimum leaf size of 10, split criterion: MSE.
   Coarse tree: 4 maximum splits, minimum leaf size of 36, split criterion: MSE.

b) *Support vector machine*
   Linear SVM: Linear kernel, box constraint level: 1, kernel scale: auto.
   Quadratic SVM: Quadratic kernel, box constraint level: 1, kernel scale: auto.
   Cubic SVM: Cubic kernel, box constraint level: 1, kernel scale: auto.

c) *Artificial neural network*
   Narrow NN: 1 hidden layer, 10 neurons, sigmoid activation function, trained using the *Scaled Conjugate Gradient* algorithm.
   Bilayered NN: 2 hidden layer, 10 neurons per layer, sigmoid activation function, trained using the *Scaled Conjugate Gradient* algorithm.

3 Results and discussion

3.1 Physisorption, surface morphology, functional group and chemical bond analysis

A physisorption analysis was performed to determine the surface and pore characteristics of the pristine OPA, acid-washed OPA (labelled as OPA), and OPA-KOH(1:2). The obtained results are presented in Table 2, which shows that the pristine OPA exhibits a low specific total surface area of 9.51 m^2/g and a high average pore size of 535.71 Å. The surface area of the pristine OPA was comparable to that reported in a previous study (10.2 m2/g) (Zainudin et al. 2005). The analysis results indicated that carbonization and chemical activation via KOH-modification have

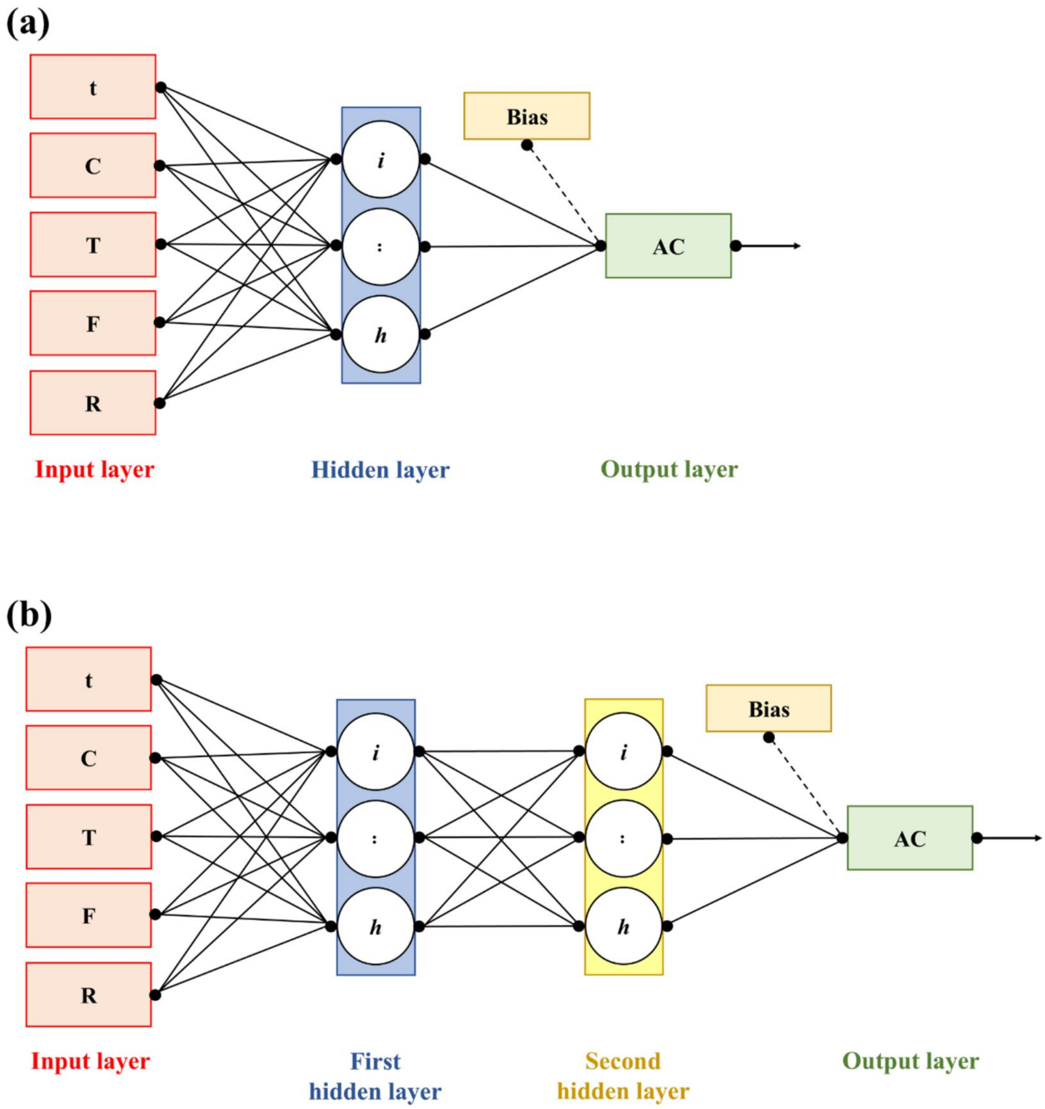

Fig. 1 Schematic diagram of the ANN model used for CO_2 adsorption modeling. **a** Single layer feed-forward NN model consisting of an input layer (red) with five parameters; time (t), CO_2 concentration (C), temperature (T), flow rate (F), and OPA-to-KOH ratio (R); connected to a single hidden layer (blue) with multiple neurons. **b** Bilayer feed-forward NN model, incorporating two hidden layers (blue and yellow). The bias neuron (yellow) adjusts the model predictions, while the output layer (green) predicts adsorption capacity (AC)

Table 2 Surface and pore characteristics of pristine OPA, OPA, and OPA-KOH(1:2)

Material	BET surface area (m^2/g)[a]	Average pore size (Å)[b]	Micropore volume (cm^3/g)[c]	Mesopore volume (cm^3/g)[c]	Macropore volume (cm^3/g)[d]
Pristine OPA	9.51	535.71	0.036	0.032	0.006
OPA	25.53	95.00	0.025	0.135	Negligible
OPA-KOH(1:2)	30.95	72.71	0.006	0.196	Negligible

[a] from BET desorption method

[b] from BJH desorption method

[c] from t-plot method

[d] is the difference between total pore volume and the total of micro- and mesopore volume

significantly improved the pore development and overall surface area of the adsorbent. Upon carbonization, the specific surface area of OPA was increased to 25.53 m2/g, more than twice the initial value, which further increased to 30.95 m2/g (KOH-activated OPA at 1:2 ratio), demonstrating the effectiveness of chemical activation in enhancing surface porosity. Moreover, after undergoing carbonization and KOH activation, the surface area of OPA-KOH(1:2) was approximately three times greater than that of the OPA sample synthesized in a previous study (Zainudin et al. 2005). This difference demonstrated the successful preparation of the adsorbent material in this study.

This study has also found that the pristine OPA predominantly exhibited macroporous structures with an average pore size of 535.71 Å. In contrast, the KOH-functionalized OPA displayed a reduced pore size in the mesoporous range, averaging at 72.71 Å, which is highly favorable for selective CO_2 capture. This result aligned with the results of previous studies that highlighted the effectiveness of KOH in enhancing pore structure and the overall surface characteristics of the adsorbents (Acquah et al. 2016; Nandi et al. 2023; Ogungbenro et al. 2020; Yağmur and Kaya 2021). These effects could be attributed to the introduction of metallic potassium into the carbon matrix, which widened the spacing between carbon atomic layers (Ganesan and Shaijumon 2016).

Figure 2 depicts the FESEM micrographs of the pristine OPA, OPA, and OPA-KOH(1:2). The surface of the pristine OPA was dense, sponge-like, and non-porous, with tiny agglomerates or clusters attached to its external surface, which indicated the presence of impurities such as ash and volatile materials. The same observation was also reported for pristine OPA in a previous study (Zainudin et al. 2005).

Figure 2b shows that the number of agglomerates on the external surface of the acid-washed OPA is visibly reduced, indicating that the contaminants and ash previously present on the surface have been removed. The activation of OPA with KOH at a high temperature leads to the formation of abundant pores in the prepared OPA-KOH(1:2), as shown in Fig. 2c. The high-temperature activation led to the development of mesopores with a well-defined structure, which enhanced the surface area and pore diameter of this sample. Additionally, the removal of volatiles contributed to a progressively less dense morphology and a reduction in particle size (Zainudin et al. 2005). The morphology of OPA-KOH(1:2), as shown in Fig. 2c, reveals a highly porous matrix with large interstitial pores. This result confirms the increase in specific surface area and the reduction in average pore diameter of this sample, as listed in Table 2.

FTIR spectroscopy was used to verify and compare the functional groups and chemical bonds in acid-washed OPA and OPA-KOH (1:2). Figure 3 shows the FTIR spectra of these samples in the range of 4000–400 cm^{-1}.

The OPA showed a peak at 3430 cm^{-1}, which could be attributed to the O–H vibrational stretching of the hydroxyl groups in the structure of the sample. The band at 783 cm^{-1} for OPA could be attributed to the *cis*-C-H out-of-plane bending of alkene structures (Coates 2000). A weak band at approximately 2383 cm^{-1} in both OPA and OPA-KOH(1:2) samples corresponded to the asymmetric stretching of CO_2, which could be present due to the adsorbed CO_2 on the surface of the porous materials. Traces of CO_2 detected in these samples could possibly be due to exposure to air. The weak bands at 1878 and 1793 cm^{-1} could be attributed to the symmetric and asymmetric C=O stretching vibrations of anhydride groups, respectively. The band detected at 783 cm^{-1} would typically be attributed to the C=C bending in alkenes. It was more pronounced in the OPA sample than in the OPA-KOH(1:2) sample, indicating a higher alkene content in the former than in the latter. In some cases, this band might also indicate adsorbed water due to the H-O-H bending vibrations

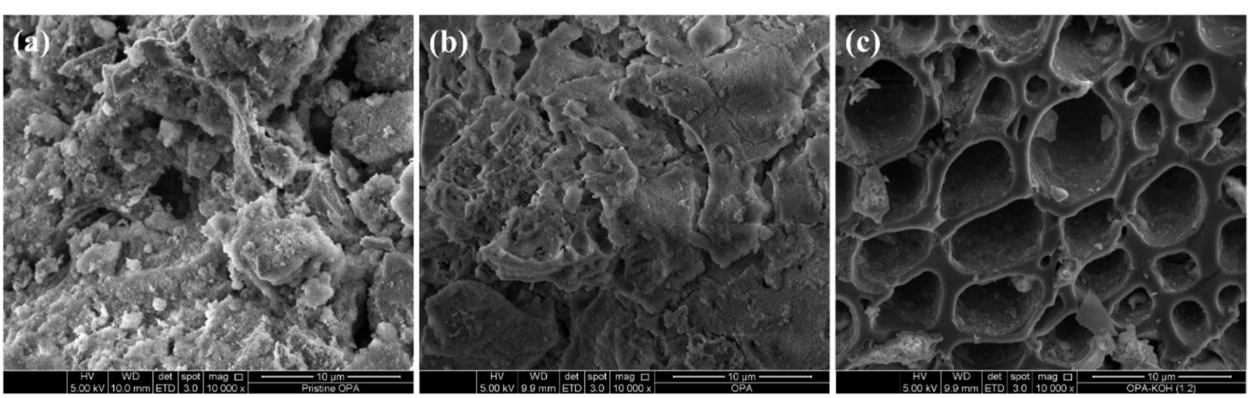

Fig. 2 FESEM micrographs of OPA samples: (**a**) pristine OPA; (**b**) OPA; and (**c**) OPA-KOH(1:2) at 10000X magnification

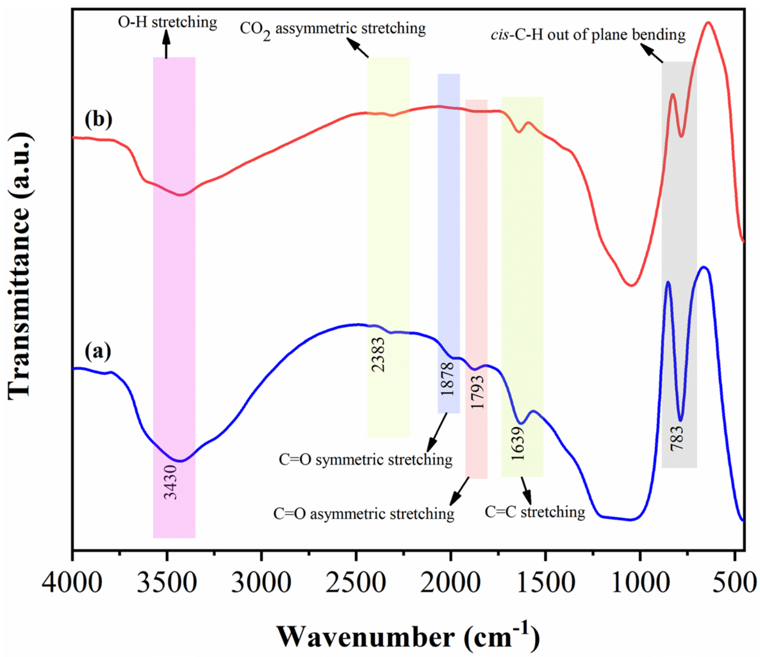

Fig. 3 FTIR spectra of (**a**) OPA and (**b**) OPA-KOH(1:2)

(Socrates 2001). As shown in Fig. 3, peaks at 1878 cm^{-1} and 1793 cm^{-1} have disappeared after KOH modification, possibly due to a reaction between hydroxyl groups and KOH during impregnation. These peaks corresponded to the C=O stretching in conjugated acid halides (Zhang et al. 2010).

3.2 Performance analysis of carbon dioxide capture

The dynamic adsorption test results, presented as breakthrough curves, were used to determine the breakthrough time (t_b), adsorption isotherm models, kinetic models, and the thermodynamic properties of the dynamic adsorption process. Figure 4a–d shows the breakthrough curves of the effects of different OPA-to-KOH ratios, flow rates, temperatures, and initial CO_2 concentrations, respectively.

To investigate the effect of KOH activation on CO_2 capture performance, samples of acid-washed OPA and KOH-activated OPA with varying OPA-to-KOH ratios (1:0.5, 1:1, 1:3, and 1:4) were tested at a flow rate of 30 mL/min, a temperature of 30 °C, and an inlet CO_2 concentration of 10 vol.%. The adsorption capacity of acid-washed OPA was 1.00 mmol/g, while the adsorption capacities of OPA-KOH(1:0.5), OPA-KOH(1:1), OPA-KOH(1:2), and OPA-KOH(1:3) were 1.41, 1.95, 2.67, and 1.48 mmol/g, respectively. Figure 4a shows that OPA-KOH(1:2) has the longest breakthrough time at approximately 6 min, indicating the highest adsorption capacity. When the OPA-to-KOH ratio was increased from 1:0.5 to 1:2, the adsorption capacity began to show an upward trend, which could be attributed to enhanced pore development and increased surface area. This observation aligned with previously reported studies on KOH-activation (Ghosh and Barron 2017; Zhang et al. 2024). However, CO_2 adsorption capacity began to decrease when OPA-KOH(1:3) was used, which could be due to the collapsed carbon structure caused by the excessive amount of KOH, leading to a reduction in accessible surface area (Ghosh and Barron 2017).

Next, to examine the effect of flow rate on CO_2 capture performance, the CO_2 adsorption capacity of OPA-KOH(1:2) was tested at different flow rates (30, 40, 50, and 60 mL/min), while keeping the initial CO_2 concentration and temperature constant at 10 vol.% and 30 °C, respectively. Notably, the highest adsorption capacity recorded was 2.67 mmol/g at a flow rate of 30 mL/min. Thus, OPA-KOH(1:2) has sufficient contact time with CO_2 for the capture to occur effectively. Whereas, at a flow rate of 60 mL/min, the breakthrough occurred faster at 1.67 min (often termed as premature breakthrough), which reduced its adsorption performance due to insufficient adsorbent-adsorbate interaction time. This was because the external film mass transfer resistance at the surface of the adsorbent began to decrease at higher flow rates, leading to reduced saturation time and CO_2 uptake (Patel 2019). The breakthrough curves in Fig. 4b also show that all adsorbents produce steeper slopes with increasing flow

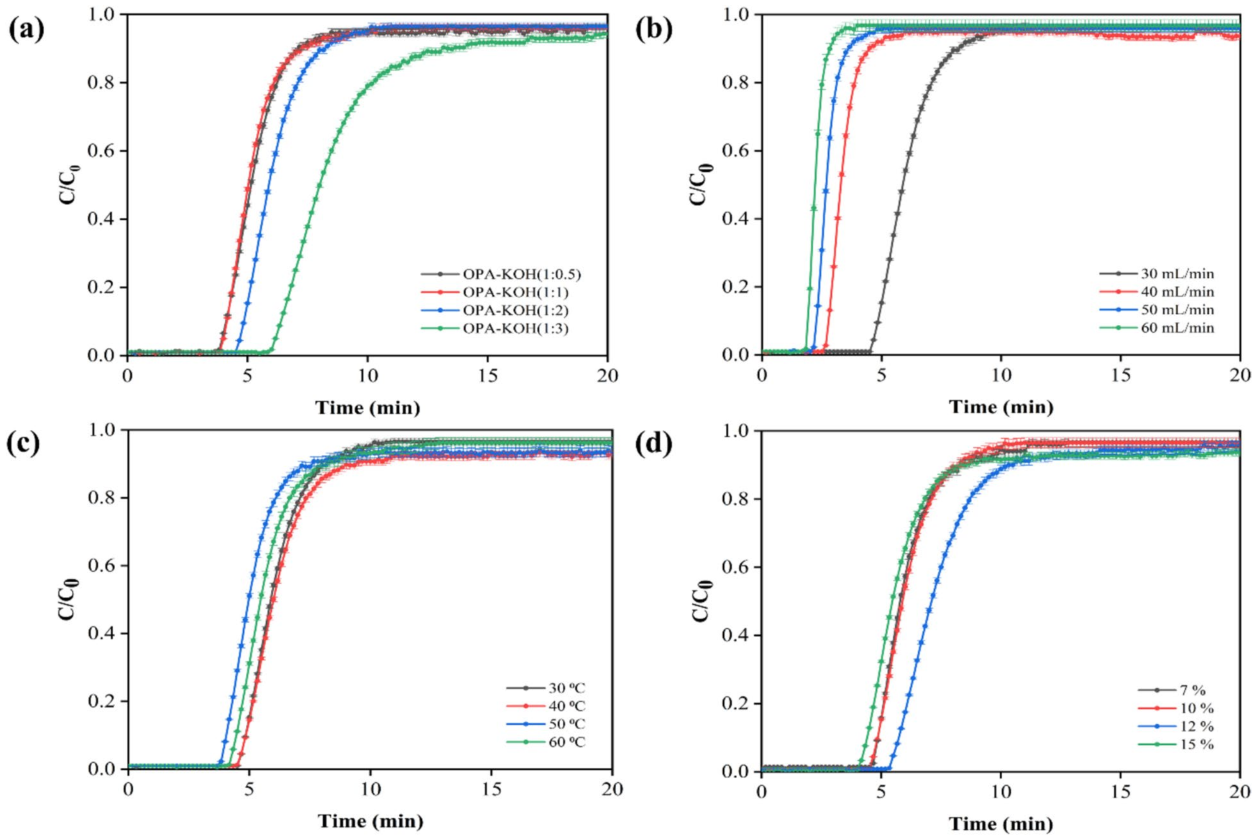

Fig. 4 CO_2 adsorption breakthrough curves: (**a**) OPA and OPA-KOH(*x*) at different OPA-to-KOH ratios; (**b**) OPA-KOH(1:2) at different flow rates; (**c**) OPA-KOH(1:2) at different temperatures; and (**d**) OPA-KOH(1:2) at different initial CO_2 concentrations

rate. This observation could be attributed to the lower mass transfer resistance at high gas flow rates (Gabelman 2017; Patel 2019). In contrary, at low gas flow rates, CO_2 molecules have sufficient residence time to diffuse into the pores of the adsorbents, resulting in relatively higher CO_2 uptakes (Patel 2019). This condition is clearly observed in the slope of the breakthrough curve for flow rate at 30 mL/min compared to the other flow rates shown in Fig. 4b.

Temperature could also have a significant impact on the efficiency and capacity of the adsorption process. This is because temperature affects how much energy the adsorbate molecules have and how they interact with the adsorbent surface. In this study, the effect of temperature was examined at 30–60 ℃, while maintaining the flow rate at 30 mL/min. The results showed that the adsorption capacity of OPA-KOH(1:2) decreased from 2.67 to 1.30 mmol/g as the temperatures increased from 30 to 60 °C. This observation demonstrated that higher temperature could negatively affect CO_2 capture performance. As observed in Fig. 4c, at the lower temperatures of 30 and 40 °C, the adsorbent takes longer to reach breakthrough, indicating a better CO_2 adsorption capacity. However, at higher temperatures (50 and 60 °C), breakthrough occurred faster, indicating reduced CO_2 uptake efficiency. At lower temperatures, physisorption was driven by the Van der Waals forces, which became more effective because the adsorbate molecules possessed reduced kinetic energy, thus facilitating their adherence to the adsorbent surface (Zhou et al. 2022). On the other hand, when the temperature was increased, these molecules could move faster and were more likely to break away from the surface, thus reducing the number of adsorbates that could effectively be adsorbed onto the surface of OPA-KOH(1:2). Another reason for these results could be attributed to the release of heat during the CO_2 adsorption process on OPA-KOH(1:2), whereby adsorption was reduced at higher temperatures because the equilibrium has shifted away from CO_2 binding (Ibrahim et al. 2022).

The effect of different CO_2 initial concentrations was examined at 7–15 vol.% while the initial flow rate of 30 mL/min and temperature of 30 °C were kept constant. The maximum adsorption capacity achieved was 2.9 mmol/g at 15 vol.% of CO_2 initial concentration, whereas the adsorption capacity at 7 vol.% of CO_2 was only 1.05 mmol/g. These results indicated that the adsorption capacity was increased with increasing CO_2 initial concentration. However, it was observed that the breakthrough curves for all prepared adsorbents retained nearly similar slopes and shapes at different CO_2 concentrations. In general, higher CO_2 concentrations could enhance the adsorption capacity of the adsorbent by increasing mass transfer, which could enable better interaction between CO_2 molecules and the adsorption sites on the adsorbent (activated carbon) (Al Mesfer and Danish 2018; Di et al. 2022). In this study, even though the highest CO_2 capture performance was recorded at the initial CO_2 concentration of 15 vol.%, the breakthrough curve at 12 vol.% showed a slightly different pattern compared to the other concentration values and exhibited the longest breakthrough time. This unexpected result could be attributed to several factors. At this concentration, the adsorption rate and gas flow rate might be balanced, which could reduce the competition among CO_2 molecules and allowed for an extended adsorption time before breakthrough (Al Mesfer and Danish 2018).

This study has established a direct correlation between synthesis conditions, adsorbent properties, and adsorption capacity, demonstrating that a balance between surface area pore size, and adsorption kinetics could be crucial in optimizing CO_2 capture. Table 3 presents a comparative analysis of CO_2 uptake performances, surface areas, and carbonization temperatures of various activated carbons derived from various biomass precursors, as reported in the literature, alongside the findings in this current study.

The tabulated summary shows that the maximum CO_2 adsorption capacity of the OPA-KOH(1:2) adsorbent in this work either surpasses or is comparable to the maximum CO_2 adsorption capacities reported for other adsorbents derived from various biomass precursors in previous studies. Table 3 also highlights the differences in process conditions and performance across various adsorbents. Although some studies have focused on developing higher surface areas, this work has focused on balancing economic feasibility, sustainability, and adsorption performance. For example, the work by Azmi and his group (Azmi et al. 2024) achieved a higher surface area (1045 m^2/g) using MgO and algae. However, the reported CO_2 adsorption capacity was not necessarily superior to that of OPA-KOH(1:2). This result reinforced the observation that adsorption efficiency was not solely determined by surface area but also by pore structure, selectivity, and functionalization. The mesoporous structure of OPA-KOH(1:2) has led to efficient CO_2 diffusion and enhanced adsorption kinetics, making it a competitive and sustainable adsorbent choice.

Table 3 Comparison of CO_2 uptake performance of activated carbons derived from various biomass sources

Biomass	Chemical activation	Carbonization temperature (^{0}C)	Surface area (m^2/g)	CO_2 uptake (mmol/g)	Ref.
Oil palm ash	KOH	700	30.95	2.9	This work
Gelatin and starch	KOH	700	1957	3.84	(Alabadi et al. 2015)
Nypha fruticans	-	400	1150.5	1.36	(Isahak et al. 2018)
	CuO	400	660.8	1.43	
Lignin	KOH	400	-	2.4	(Huang et al. 2019)
Garlic peel	-	800	306	1.65	(Huang et al. 2019)
	KOH	800	1206	2.82	
Sugar bagasse	-		3.5	1.66	(Han et al. 2019)
	Urea		32	1.94	
Olive stone	-	700	6.4	3.74	(Puig-Gamero et al. 2021)
Hazelnut shell	KOH	500	11.18	3.97	(Pang et al. 2021)
Chitosan	-	300	2149	2.97	(Wang et al. 2021)
Glucose	$KHCO_3$ and urea	800	1769	4.26	(Shi et al. 2022)
Rice husk	KOH	450	1439	1.39–2.55	(Wang et al. 2022)
	K_2CO_3	450	-	3.33	
Coconut shell	-	700	976	1.75	(Azmi et al. 2024)
	MgO and algae	700	1045	2.65	
Olive pomace	KOH	650	986	3.1	(Alcazar-Ruiz et al. 2024)

Table 4 Isotherm model parameters for CO_2 adsorption using OPA-KOH(1:2)

Model parameters	Temperature (^oC)			
	30	40	50	60
Langmuir isotherm				
q_{max} (mg/g)	113.030	78.690	65.732	55.276
k_L (L/mg)	4.669	3.949	3.809	6.168
R^2	0.998	0.990	0.986	0.994
X^2	2.220	1.181	1.193	1.199
Freundlich isotherm				
k_F (mg/g)/(L/mg)$^{1/n}$	186.175	137.772	122.222	93.379
n_F	4.243	3.789	3.693	4.903
R^2	0.998	0.998	0.982	0.995
X^2	1.994	0.934	1.048	1.161

3.3 Theoretical modeling of CO_2 adsorption behavior

3.3.1 Adsorption isotherm analysis

In general, isotherm models can provide insights into equilibrium behavior and CO_2 adsorption capacity. To analyze the CO_2 adsorption profile of OPA-KOH(1:2), the parameters for the Langmuir and Freundlich models were fitted to the experimental datasets. Non-linear regression fitting is applied to determine the parameters of both models, along with the correlation coefficients (R^2) and chi-squared error (X^2) for CO_2 adsorption, as detailed in Table 4. The fundamental idea of the Langmuir isotherm model is that adsorption occurs on a uniform surface with identical adsorption sites, making it applicable to homogeneous surfaces (Langmuir 1918). In contrast, the Freundlich isotherm provides a practical equation that accounts for non-ideal adsorption processes on heterogeneous surfaces with varying adsorption energies (Ammendola et al. 2017; Freundlich 1906).

The results in Table 5 show that the Freundlich isotherm is the best fit for describing CO_2 adsorption onto OPA-KOH(1:2), with R^2 values ranging from 0.982 to 0.998, and low X^2 values ranging from 0.934 to 1.994 across all temperatures. This table indicates that CO_2 adsorption onto OPA-KOH(1:2) is heterogeneous by nature. Moreover, the values of the calculated separation factor (R_L) at different temperatures, as shown in Table 5, are all less than 1, which confirms that CO_2 uptake is favorable using OPA-KOH(1:2). These findings aligned with the findings of a previous study on KOH-activated biomass-derived adsorbents, which also reported Freundlich-type adsorption behaviour for CO_2 capture (Wang et al. 2022).

Table 5 Separation factors of CO_2 adsorption using OPA-KOH(1:2)

Temperature (^oC)	Separation factor, R_L
30	0.02097
40	0.02470
50	0.02558
60	0.01596

Figure 5 shows the experimental results and the predictions made using the Langmuir and Freundlich isotherm models across all temperatures using OPA-KOH(1:2). It shows that non-linear regression for the Langmuir isotherm is suboptimal for analyzing CO_2 adsorption onto OPA-KOH(1:2), while the Freundlich isotherm is an excellent fit for the experimental data. As shown in Table 4, the k_F value decreases with increasing temperature, while the n_F values at all temperatures are greater than 1. These results indicated the CO_2 adsorption onto OPA-KOH(1:2) was primarily driven by physisorption rather than chemisorption. Thus, this multilayer adsorption mechanism was more prevalent in OPA-KOH(1:2), which indicated the enhanced accessibility of CO_2 molecules deep into the adsorbent's pores in the presence of numerous adsorption sites, with minimal chemical adsorption. Hence, this finding indicated that CO_2 molecules could interact with numerous adsorption sites of varying strengths rather than forming a single uniform layer, as seen in the Langmuir model (Gautam et al. 2023). Similar findings have been reported in previous studies (Melouki et al. 2020; Serafin et al. 2017).

3.3.2 Adsorption kinetic analysis

The adsorption rate was crucial for evaluating the CO_2 uptake mechanism (Ruthven 1984) of the OPA-KOH(1:2) adsorbent and the rate at which the adsorbate-adsorbent interaction occurred. In this research, adsorption kinetics was analyzed using non-linear regression to fit the pseudo-first order and pseudo-second order kinetic models. Table 6 presents the calculated parameters for these models, providing insight into the kinetics of the adsorption process. Meanwhile, Fig. 6 illustrates the experimental data alongside the predictions made using these kinetic models across all temperatures for OPA-KOH(1:2).

The analysis results of the kinetic data showed that the pseudo-second-order kinetic model was a more suitable fit for CO_2 adsorption using OPA-KOH(1:2), with R^2 values of greater than 0.99 and X^2 values of less than 0.397. However, at the lower temperature of 30 °C, the experimental data showed a better fit with the pseudo-first order kinetic model. Similar behaviors have been reported for various chemically activated ACs, where adsorption rates were primarily governed by surface diffusion and weak electrostatic interactions (Azmi et al.

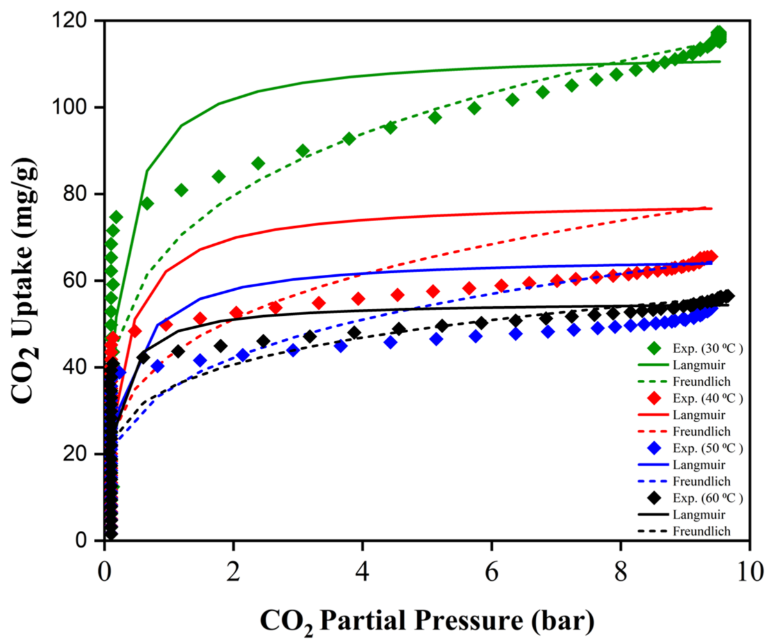

Fig. 5 Nonlinear isothermal model fitting for experimental vs. predicted CO_2 adsorption capacities of OPA-KOH(1:2)

Table 6 Parameters of kinetic models for CO_2 adsorption using OPA-KOH(1:2)

Model parameters	Temperature (°C)			
	30	40	50	60
Pseudo-first order model				
$q_{e,exp}$ (mg/g)	117.367	82.058	65.383	56.254
$q_{e,calc}$ (mg/g)	139.099	82.005	68.181	61.834
k_1 (1/min)	0.207	0.153	0.156	0.249
R^2	0.998	0.993	0.988	0.997
X^2	0.278	0.275	0.382	0.112
Pseudo-second order model				
$q_{e,exp}$ (mg/g)	117.367	82.058	65.383	56.254
$q_{e,calc}$ (mg/g)	203.227	94.403	78.787	83.515
K_2 (1/min)	0.001	0.002	0.003	0.003
R^2	0.990	0.998	0.997	0.993
X^2	0.397	0.105	0.148	0.200

2024; Serafin et al. 2017; Serafin and Dziejarski 2023). Although some data points in Fig. 6 are slightly overestimated, they remain reasonably close to the experimental values and could be considered an excellent fit.

Table 6 shows an increase in K_2 values from 30 to 50 °C, while at 60 °C, the value remains the same. These different trends indicated that the diffusion rate of CO_2 into the pores of OPA-KOH(1:2) was increased with increasing temperature (Shao et al. 2022). However, the adsorption mechanism could not be conclusively established solely through kinetic experiments or kinetic models fitting per se. These models could only predict the adsorption behaviour for a specific adsorbent-adsorbate interaction under specific operating parameters. Any slight modification to the structure or characteristics of the adsorbent, or even to the properties of the adsorbate could alter the adsorption mechanism and, consequently, affect the adsorption kinetics.

3.3.3 Adsorption thermodynamic analysis

The fundamental thermodynamic parameters, namely $\triangle G°$, $\triangle H°$, and $\triangle S°$ have been used to evaluate the feasibility of the adsorption process and to analyze its energetics. The values of these parameters have been summarized in Table 7.

The values of $\triangle G°$ were consistently negative across all temperatures, indicating that the CO_2 adsorption could be classified as thermodynamically favorable and spontaneous. Consequently, CO_2 adsorption onto OPA-KOH(1:2) adsorbent was primarily classified as physisorption, together with weak chemisorption effects (Azmi et al. 2024). However, the value of $\triangle G°$ began to increase with increasing temperature, indicating a diminishing driving force for the adsorption process and a lower tendency for it to occur spontaneously (Pacześniak et al. 2018). The $\triangle H°$ value for CO_2 adsorption onto OPA-KOH(1:2) was also negative, indicating that the adsorption process was exothermic and involved the release of energy. The $\triangle S°$ value indicated a decrease in the entropy of CO_2 molecules during the adsorption process. Initially,

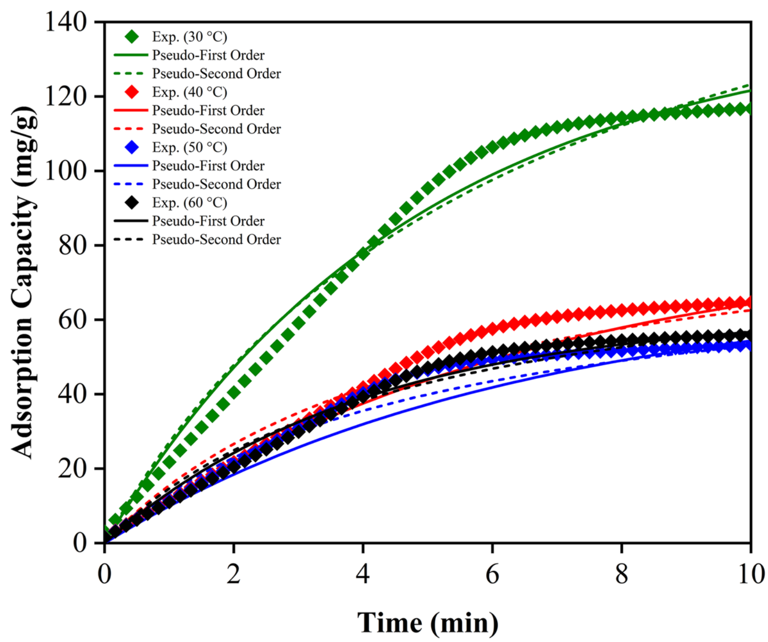

Fig. 6 Nonlinear kinetic model fitting for experimental vs. predicted CO_2 adsorption capacities of OPA-KOH(1:2)

CO_2 molecules exhibited irregular motions due to their gaseous state. However, upon adsorption onto OPA-KOH(1:2), they became more orderly arranged. In conclusion, negative $\triangle G°$, $\triangle H°$, and $\triangle S°$ values were observed across all temperatures under standard operating conditions, which indicated that the adsorption of CO_2 was spontaneous and primarily driven by enthalpy.

3.4 Plausible adsorption mechanism

Figure 7 illustrates a viable CO_2 capture mechanism using OPA-KOH(1:2) to provide insight into the interactions governing this process. Based on the isothermal, kinetic, and thermodynamic analyses, it can be concluded that the adsorption of CO_2 onto OPA-KOH(1:2) was primarily governed by physical adsorption, with the possibility of weak chemical interactions occurring simultaneously. This conclusion was based on further analysis of the CO_2 adsorption kinetics, which implied that chemisorption could have played a minor role due to the presence of surface functional groups (i.e., -OH, -COO^-, K^+) introduced during KOH activation. These functional groups could have enhanced CO_2 uptake via weak electrostatic interactions between CO_2 molecules and the carbon surface of the adsorbent (El-Desouky et al. 2022).

Furthermore, the highly porous structure of OPA-KOH(1:2), as shown in the FESEM image in Fig. 2c, facilitates the physical adsorption of CO_2 through weak Van der Waals forces at the surface layer. The pore structure of OPA also played a crucial role in CO_2 adsorption. Micropores (< 2 nm) primarily contribute to physisorption, whereby CO_2 molecules are trapped due to Van der Waals forces, while mesopores (2–50 nm) provide pathways for rapid diffusion and enhanced surface contact (Serafin et al. 2017). As shown in Fig. 7, CO_2 molecules could move from macropores to mesopores and then to micropores until all pores are fully occupied. Electrostatic forces of attraction, including diffusive adsorption, could also contribute to the overall CO_2 adsorption efficiency. The negatively charged sites on OPA-KOH(1:2), due to the presence of hydroxyl ions in KOH molecules, and the partial charges on CO_2 molecules could lead to electrostatic forces of attraction. These observations are further supported by the presence of the O–H vibrational stretching peak at 3430 cm^{-1} in the OPA-KOH(1:2) material, as indicated by the FTIR spectra in Fig. 3. The hydroxyl functional groups of KOH molecules in OPA-KOH(1:2) could also interact with oxygen atoms in the CO_2 molecules through hydrogen bonding. The physical and chemical interactions that occurred during the CO_2 adsorption process have highlighted the complexity of this process. Therefore,

Table 7 Thermodynamic parameters for CO_2 adsorption using OPA-KOH(1:2)

Temperature (°C)	ΔG^0 (kJ/mol)	ΔH^0 (kJ/mol)	ΔS^0 (kJ/mol.K)
30	−13.174	−18.395	−0.017
40	−12.824		
50	−12.912		
60	−12.566		

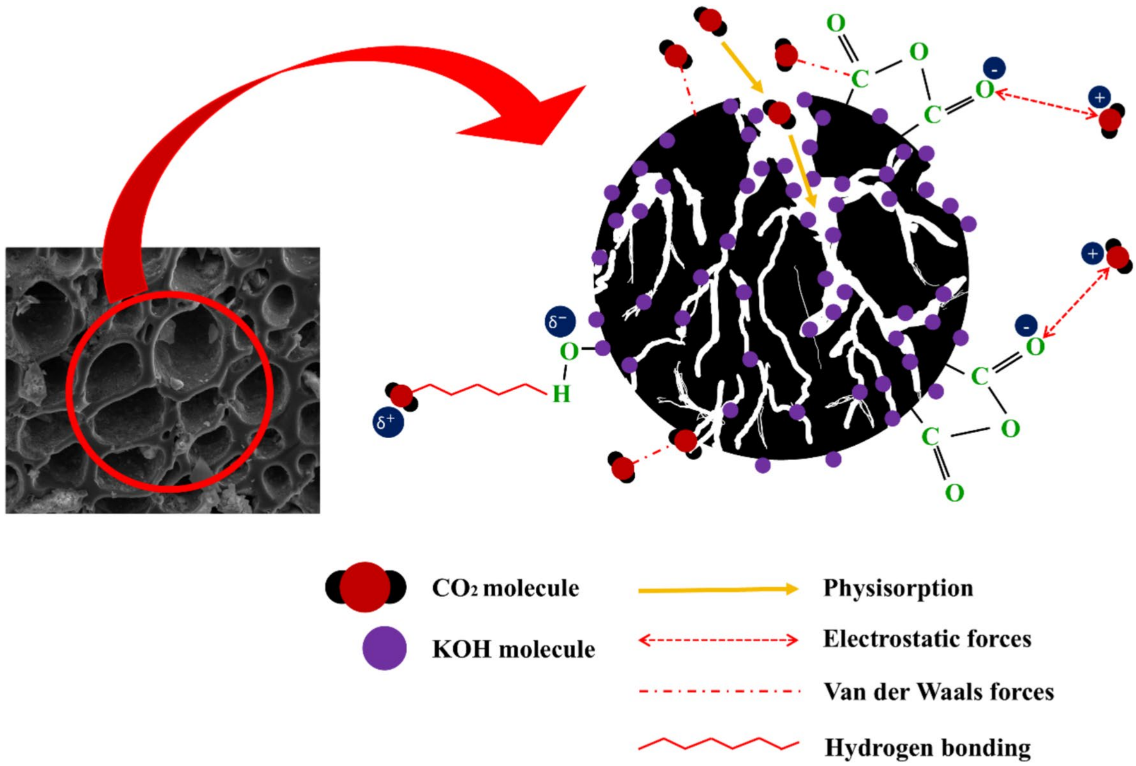

Fig. 7 Plausible CO_2 adsorption mechanism onto OPA-KOH(1:2)

Table 8 Statistical analyses of the ML-based models

Model	RMSE	MSE	R^2	MAE
Fine DT	0.1557	0.0243	0.9439	0.0913
Coarse DT	0.3780	0.1429	0.6695	0.3002
Medium DT	0.2684	0.0721	0.8333	0.1742
Linear SVM	0.4172	0.1741	0.5974	0.2522
Quadratic SVM	0.3191	0.1018	0.7645	0.1979
Cubic SVM	0.2446	0.0598	0.8616	0.1648
Narrow NN	0.0856	0.0073	0.9831	0.0470
Bilayered NN	0.0470	0.0022	0.9949	0.0224

experimental investigations are crucial for understanding and optimizing the intricate interplay of adsorbate-adsorbent interactions for enhanced CO_2 uptake performance. This combined mechanism aligned with the mechanism proposed by previous studies on KOH-activated ACs (Azmi et al. 2024).

3.5 Machine learning-based models

Table 8 summarizes the statistical comparison of the performances of different ML models, including DT, SVM, and NN. These models were evaluated based on standard statistical metrics, namely, root mean square error (RMSE), mean square error (MSE), coefficient of determination (R^2), and mean absolute error (MAE). Figure 8 shows the regression plots for all ML models, by comparing the scattering of residuals of the experimental responses to the perfect predictions.

Based on the results presented in Table 8, the bilayered NN demonstrates superior accuracy among the tested models, by achieving the lowest RMSE (0.0470), MSE (0.0022), and MAE (0.0224) values, along with the highest R^2 value (0.9949). These results indicated the excellent predictive capability of the bilayered NN model for the dataset in this study. Table 8 also shows that the narrow NN performs quite well but is lightly underperforming compared to the bilayered NN. In contrast, the linear SVM and the coarse DT models exhibited extremely poor performances, with low R^2 values of 0.5974 and 0.6695, respectively, and higher errors, suggesting their limitations in capturing the complex relationships in the dataset.

The x-axis in Fig. 8 represents the true response that corresponds to the actual CO_2 adsorption capacity, while the y-axis represents the predicted response, corresponding to the predicted CO_2 adsorption capacity.

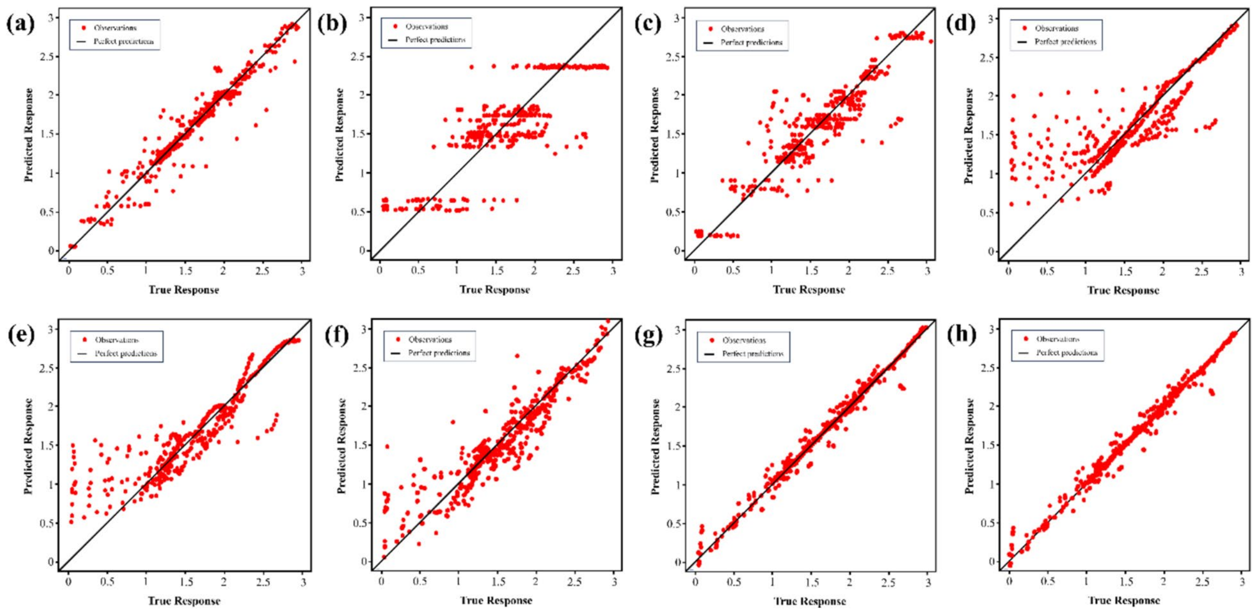

Fig. 8 Regression plots for different ML-based models

The closer the data points were to the diagonal line (perfect prediction line), the stronger the model's predictive ability. Based on Fig. 8, the bilayered NN demonstrates the closest alignment to the perfect prediction line, which further validates its accuracy. Most output data aligned well with the target data, as indicated by the extensive distribution of data points along the perfect prediction line with minimal disparity. The evenly scattered data points along the diagonal line showed that this model was sufficiently excited by input perturbations. In contrast, the other models, namely the Coarse DT, Medium DT, Linear SVM, and Quadratic SVM, as shown in Fig. 8b-e, exhibit significant deviations from the perfect prediction line, thus indicating a lack of precision in their predictions in capturing the dataset. Meanwhile, the cubic SVM model, as shown in Fig. 8f performs moderately well in capturing the dataset but fell short compared to the NN-based models. Hence, the regression plots have demonstrated that the predictive ability of the bilayered NN was superior to that of the other ML-based models. The time-dependent simulation results for the OPA-to-KOH ratios, flow rates, temperatures, and initial concentrations are depicted in Fig. 9a–d, respectively.

The simulation results in Fig. 9 have confirmed the ability of the bilayered NN model to successfully reproduce the experimental dataset of CO_2 adsorption capacity using OPA-KOH(1:2) adsorbent. This model could accurately reflect the overall adsorption trends under varying operating parameters. This observations aligned with the results of a previous study (Pacześniak et al. 2018), which concluded that an NN model, with eight hidden nodes, has exhibited excellent capability in fitting nonlinear process datasets. Therefore, this current study has concluded that the bilayered NN model is suitable for implementation as a predictive tool of CO_2 uptake performance in future studies. Furthermore, to interpret the influence of each parameter on the predictions of this ML model, an assessment of its responses to varying process conditions was conducted. Among the studied parameters, initial CO_2 concentration showed the highest impact on CO_2 adsorption capacity, as an increase in concentration could enhance mass transfer and surface interaction. The second most influential factor was flow rate, where higher flow rates could reduce adsorption efficiency due to insufficient contact time between CO_2 molecules and the adsorbent surface. Temperature exhibited a moderate influence, with adsorption decreasing at elevated temperatures due to the exothermic nature of the process. The OPA-to-KOH ratio played a minor but significant role, primarily affecting porosity and surface area development, which subsequently influenced adsorption capacity. These analyses have highlighted that ML models could effectively capture the nonlinear interactions between these parameters, reinforcing their predictive capability for optimizing CO_2 adsorption performance. In short, the findings in this study showed that oil palm ash-derived activated carbon has the potential as the adsorbent for large-scale CO_2 capture applications. The integration of ML models for adsorption predictions could facilitate real-time process monitoring, thereby enhancing efficiency in industrial applications.

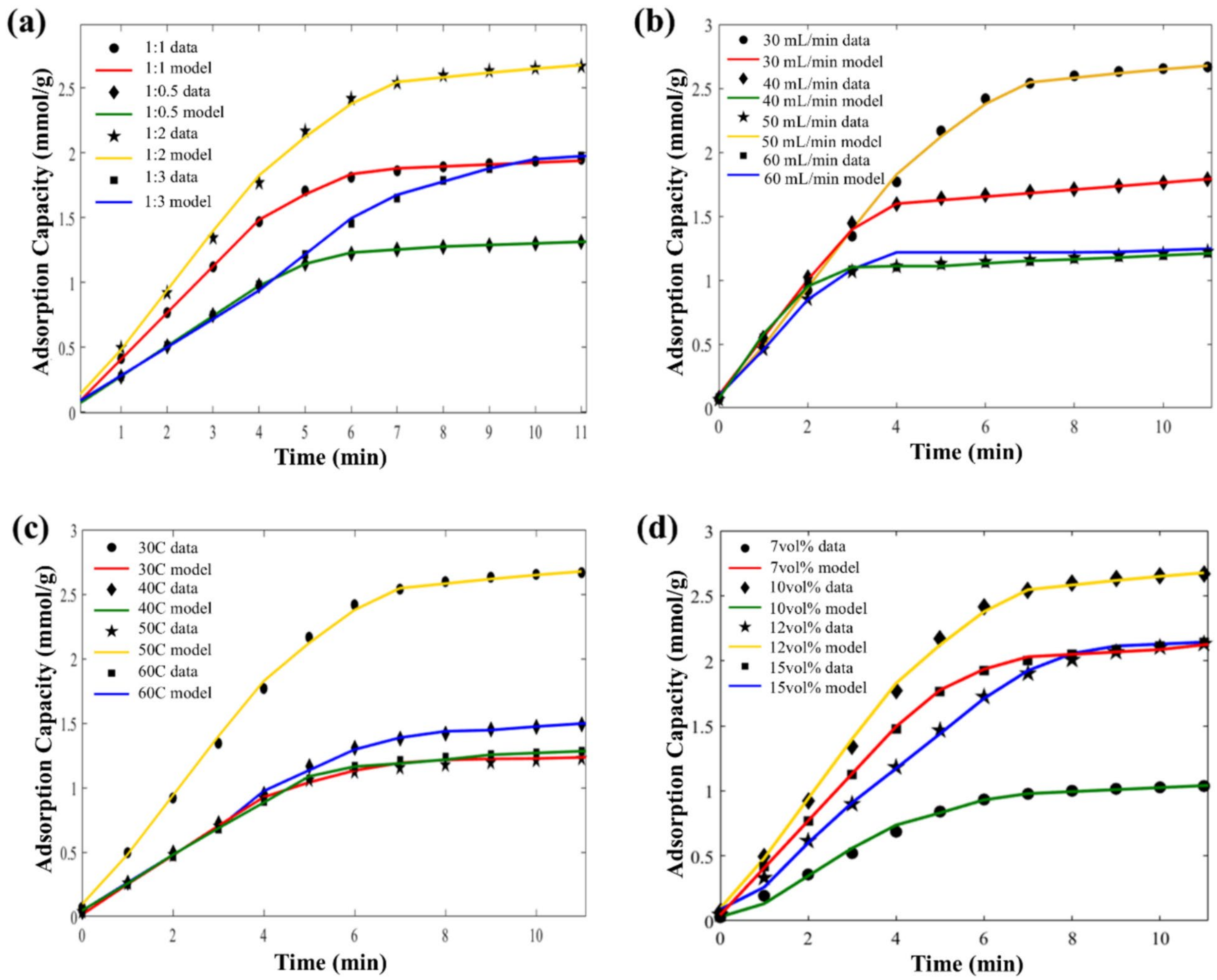

Fig. 9 Simulation results of the bilayered NN model for CO_2 adsorption under different operating parameters: (**a**) OPA-to-KOH ratios; (**b**) flow rates; (**c**) temperatures; and (**d**) initial concentrations

4 Conclusion

This study has successfully demonstrated that KOH-functionalized OPA adsorbents could be effectively utilized for CO_2 capture. The characterization results revealed that OPA-KOH(1:2) exhibited a higher surface area and smaller total average pore size compared to the pristine OPA, which have enhanced its CO_2 capture efficiency. The highest CO_2 adsorption capacity was 2.9 mmol/g using OPA-KOH(1:2) at 30 °C, flow rate of 30 mL/min, and an initial CO_2 concentration of 15 vol.%. The Freundlich isotherm model has provided the best fit for the experimental CO_2 uptake data, which suggested that the adsorption process occurred on a heterogeneous surface rather than forming a uniform monolayer. Additionally, CO_2 adsorption using OPA-KOH(1:2) followed the pseudo-second order kinetics, which indicated that this process was primarily driven by physical adsorption, supported by weak chemical interactions. This observation reinforced the assumption that surface functional groups introduced during KOH activation played a role in adsorption interactions. The thermodynamic analyses consistently yielded negative values for $\triangle G°$, $\triangle H°$, and $\triangle S°$, which confirmed that the adsorption process was thermodynamically favorable, spontaneous, and exothermic across the investigated temperature range (30–60 °C). Although numerous studies have reported ACs with higher surface areas, the adsorption efficiency of an adsorbent is not determined solely by its surface area but also by its pore structure, functional groups, and adsorption mechanism. The mesoporous nature of OPA-KOH(1:2) has facilitated effective CO_2 diffusion and accessibility to active sites, making it a viable adsorbent for CO_2 capture applications. Additionally, the economic feasibility, sustainability, and low-cost synthesis of OPA-KOH(1:2) would make it a competitive candidate for large-scale carbon capture technologies, particularly in regions with abundant oil palm waste resources. ML-based modeling has shown that the bilayered NN model has the highest accuracy in predicting CO_2, thus outperforming other ML models. Overall, the findings in this work have highlighted the potential of ML-driven approaches for accelerating CO_2 adsorption process development by providing rapid, and accurate predictive frameworks that could minimize experimental trial-and-error. The successful integration of experimental adsorption data with ML-based modeling could bridge the gap between empirical studies and advanced computational modeling, offering a scalable, data-driven solution for optimizing CO_2 capture efficiency. Beyond their laboratory-scale significance, the findings of this study have practical implications for large-scale industrial CO_2 capture applications. The utilization of agricultural waste-derived activated carbons aligns with circular economy principles, with the transformation of a low-value byproduct into a high-performance adsorbent. Given that CO_2 capture technologies play a critical role in decarbonization strategies, this work could contribute towards advancing sustainable materials for various industries, such as the cement, steel, petrochemical, and power generation sectors. The adaptability of ML-based predictive modeling could further enable real-time process control and optimization, thus enhancing industrial feasibility and economic viability. This study underscores the importance of integrating ML with materials science to develop more efficient, adaptable, and cost-effective CO_2 capture technologies, and provide a sustainable pathway for addressing global carbon emissions. Future research should explore alternative activation agents to further enhance OPA-based adsorbents, conduct long-term stability studies for industrial feasibility, and expand ML models for real-world CO_2 capture scenarios. Additionally, integrating OPA with other porous materials could optimize its adsorption performance.

Generative AI use statement
During the preparation of this work the authors used ChatGPT and Wordtune to improve the scientific writing tone and style. After using this tool/service, the authors reviewed and edited the content as needed and will take full responsibility for the content of the publication.

Authors' contributions
All authors contributed to the study conception and design. Material preparation, data collection, and analysis were performed by Syamima Nasrin Mohamed Saleh, Fakhrony Sholahudin Rohman, Dinie Muhammad, and Syafini Mohd Hussin. The first draft of the manuscript was written by Syamima Nasrin Mohamed Saleh, and all authors commented on previous version of the manuscript. Writing, review, and editing were contributed by Bassim H. Hameed, Chew Thiam Leng, and Azam Taufik Mohd Din. Supervision and funding acquisition were carried out by Azam Taufik Mohd Din. All authors read and approved the final manuscript.

Funding
This research work is fully funded by the Ministry of Higher Education Malaysia under the Fundamental Research Grant Scheme (FRGS/1/2023/TK05/USM/02/4).

Data availability
Data will be made available upon request.

Declarations

Competing interests
The authors declare that they have no known competing financial and non-financial interests that could influence the work reported in this paper.

Author details
[1]School of Chemical Engineering, Universiti Sains Malaysia, Engineering Campus, Nibong Tebal, Pulau Pinang 14300, Malaysia. [2]Process Systems Engineering Centre (UTM-PROSPECT), Research Institute of Sustainable Environment (RISE), Universiti Teknologi Malaysia, Johor Bahru, Johor 81310, Malaysia. [3]Faculty of Chemical and Energy Engineering, Universiti Teknologi Malaysia, Johor Bahru, Johor 81310, Malaysia. [4]Department of Chemical Engineering, College of Engineering, Qatar University, P.O. Box 2713, Doha, Qatar. [5]Department of Chemical Engineering, Faculty of Engineering, Universiti Teknologi PETRONAS, Seri Iskandar, Perak 32610 , Malaysia.

Received: 30 January 2025 Revised: 2 June 2025 Accepted: 4 June 2025
Published online: 18 August 2025

References
Abuelnoor N, AlHajaj A, Khaleel M, Vega LF, Abu-Zahra MRM (2021) Activated carbons from biomass-based sources for CO_2 capture applications. Chemosphere 282:131111. https://doi.org/10.1016/j.chemosphere.2021.131111
Acquah C, Yon LS, Tuah Z, Ngee NL, Danquah MK (2016) Synthesis and performance analysis of oil palm ash (OPA) based adsorbent as a palm oil bleaching material. J Clean Prod 139:1098–1104. https://doi.org/10.1016/j.jclepro.2016.09.004
Aisheh YIA (2023) Palm oil fuel ash as a sustainable supplementary cementitious material for concrete: A state-of-the-art review. Case Stud Constr Mater 18:e01770. https://doi.org/10.1016/j.cscm.2022.e01770
Al Mesfer MK, Danish M (2018) Breakthrough adsorption study of activated carbons for CO_2 separation from flue gas. J Environ Chem Eng 6:4514–4524. https://doi.org/10.1016/j.jece.2018.06.042
Alabadi A, Razzaque S, Yang Y, Chen S, Tan B (2015) Highly porous activated carbon materials from carbonized biomass with high CO_2 capturing capacity. Chem Eng J 281:606–612. https://doi.org/10.1016/j.cej.2015.06.032
Alcazar-Ruiz A, Maisano S, Chiodo V, Urbani F, Dorado F, Sanchez-Silva L (2024) Enhancing CO_2 capture performance through activation of olive pomace biochar: A comparative study of physical and chemical methods. Sustain Mater Technol 42:e01177. https://doi.org/10.1016/j.susmat.2024.e01177
Ali SA, Shah SN, Shah MUH, Younas M (2023) Synthesis and performance evaluation of copper and magnesium-based metal organic framework supported ionic liquid membrane for CO_2/N_2 separation. Chemosphere 311:136913. https://doi.org/10.1016/j.chemosphere.2022.136913
Ammendola P, Raganati F, Chirone R (2017) CO_2 adsorption on a fine activated carbon in a sound assisted fluidized bed: Thermodynamics and kinetics. Chem Eng J 322:302–313. https://doi.org/10.1016/j.cej.2017.04.037
Azmi NZM, Buthiyappan A, Patah MFA, Rashidi NA, Raman AAA (2024) Enhancing the CO_2 adsorption with dual functionalized coconut shell-hydrochar using Chlorella microalgae and metal oxide: Synthesis, physicochemical properties & mechanism evaluations. J Clean Prod 463:142736. https://doi.org/10.1016/j.jclepro.2024.142736
Bai J, Huang J, Jiang Q, Jiang W, Demir M, Kilic M, Altay BN, Wang L, Hu X (2023a) Synthesis and characterization of polyphenylene sulfide resin-derived S-doped porous carbons for efficient CO_2 capture. Colloids Surfaces A Physicochem Eng Asp 674:131916. https://doi.org/10.1016/j.colsurfa.2023.131916

Bai J, Huang J, Yu Q, Demir M, Kilic M, Altay BN, Hu X, Wang L (2023b) N-doped porous carbon derived from macadamia nut shell for CO_2 adsorption. Fuel Process Technol 249:107854. https://doi.org/10.1016/j.fuproc.2023.107854

Bai J, Shao J, Yu Q, Demir M, Altay BN, Ali TM, Jiang Y, Wang L, Hu X (2024) Sulfur-doped porous carbon Adsorbent: A promising solution for effective and selective CO_2 capture. Chem Eng J 479:147667. https://doi.org/10.1016/j.cej.2023.147667

Chatterjee S, Jeevanandham S, Mukherjee M, Vo DVN, Mishra V (2021) Significance of re-engineered zeolites in climate mitigation: A review for carbon capture and separation. J Environ Chem Eng 9:105957. https://doi.org/10.1016/j.jece.2021.105957

Chen O, Tapia VG, Rogé A et al. (2023) CO_2 emissions in 2022. International Energy Agency Official Web. https://iea.blob.core.windows.net/assets/3c8fa115-35c4-4474-b237-1b00424c8844/CO2Emissionsin2022.pdf. Accessed 5 Nov 2024

Coates J (2000) Interpretation of infrared spectra, A practical approach. John Wiley & Sons, England

Czerwinska N, Giosuè C, Matos I, Sabbatini S, Ruello ML, Bernardo M (2024) Development of activated carbons derived from wastes: Coffee grounds and olive stones as potential porous materials for air depollution. Sci Total Environ 914:169898. https://doi.org/10.1016/j.scitotenv.2024.169898

Das A, Peu SD, Hossain MS, Nahid MMA, Karim FR, Chowdhury H, Porag MH, Argha DBP, Saha S, Islam ARMT, Salah MM, Shaker A (2023) Advancements in adsorption based carbon dioxide capture technologies: A comprehensive review. Heliyon 9:e22341. https://doi.org/10.1016/j.heliyon.2023.e22341

Di J, Ruan Z, Zhang S, Dong Y, Fu S, Li H, Jiang G (2022) Adsorption behaviors and mechanisms of Cu^{2+}, Zn^{2+} and Pb^{2+} by magnetically modified lignite. Sci Rep 12:1–18. https://doi.org/10.1038/s41598-022-05453-y

El-Desouky MG, Shahat A, El-Bindary AA, El-Bindary MA (2022) Description, kinetic and equilibrium studies of the adsorption of carbon dioxide in mesoporous iron oxide nanospheres. Biointerface Res Appl Chem 12:1022–1038. https://doi.org/10.33263/BRIAC121.10221038

Fatima SS, Borhan A, Ayoub M, Ghani NA (2023) Modeling of CO_2 adsorption on surface-functionalized rubber-seed shell activated carbon: Isotherm and kinetic analysis. Processes 11:2833. https://doi.org/10.3390/pr11102833

Fierro V, Muñiz G, Basta AH, El-Saied H, Celzard A (2010) Rice straw as precursor of activated carbons: Activation with ortho-phosphoric acid. J Hazard Mater 181:27–34. https://doi.org/10.1016/j.jhazmat.2010.04.062

Freundlich HMF (1906) Over the adsorption in solution. J Phys Chem 57:385–470 (https://www.scirp.org/reference/referencespapers?referenceid=857464)

Gabelman A (2017) Adsorption basics: Part 2. Chem Eng Prog 113:1–6. https://www.aiche.org/sites/default/files/docs/pages/adsorption_basics_part_2.pdf

Ganesan A, Shaijumon MM (2016) Activated graphene-derived porous carbon with exceptional gas adsorption properties. Microporous Mesoporous Mater 220:21–27. https://doi.org/10.1016/j.micromeso.2015.08.021

Gautam R, P, Sahoo, S, (2023) A review on adsorption isotherms and kinetics of CO_2 and various adsorbent pairs suitable for carbon capture and green refrigeration applications. Sadhana Academy Proc Eng Sci 48:27. https://doi.org/10.1007/s12046-023-02080-9

Gayathiri M, Pulingam T, Lee KT, Sudesh K (2022) Activated carbon from biomass waste precursors: Factors affecting production and adsorption mechanism. Chemosphere 294:133764. https://doi.org/10.1016/j.chemosphere.2022.133764

Ghosh S, Barron AR (2017) The effect of KOH concentration on chemical activation of porous carbon sorbents for carbon dioxide uptake and carbon dioxide-methane selectivity: The relative formation of micro- (<2 nm): Versus meso- (>2 nm) porosity. Sustain Energy Fuels 1:806–813. https://doi.org/10.1039/c6se00102e

González B, Manyà JJ (2020) Activated olive mill waste-based hydrochars as selective adsorbents for CO_2 capture under postcombustion conditions. Chem Eng Process- Process Intensif 149:107830. https://doi.org/10.1016/j.cep.2020.107830

Guo Y, Tan C, Sun J, Li W, Zhang J, Zhao C (2020) Porous activated carbons derived from waste sugarcane bagasse for CO_2 adsorption. Chem Eng J 381:122736. https://doi.org/10.1016/j.cej.2019.122736

Han J, Zhang L, Zhao B, Qin L, Wang Y, Xing F (2019) The N-doped activated carbon derived from sugarcane bagasse for CO_2 adsorption. Ind Crops Prod 128:290–297. https://doi.org/10.1016/j.indcrop.2018.11.028

Huang GG, Liu YF, Wu XX, Cai JJ (2019) Activated carbons prepared by the KOH activation of a hydrochar from garlic peel and their CO_2 adsorption performance. New Carbon Mater 34:247–257. https://doi.org/10.1016/S1872-5805(19)60014-4

Huang K, Du X, Li K, Zhou J, Zhang D, Abbas N, Cheng Y, Wu T, Liu G, He C (2024) Competitive adsorption of CO_2/CH_4 on coal: Insights from thermodynamics. Alexandria Eng J 97:114–126. https://doi.org/10.1016/j.aej.2024.04.010

Ibrahim M, Hameed BH, Ouakouak A, Din ATM (2022) Effect of hydrothermal carbonization parameters and performance of carbon dioxide adsorption on pineapple peel waste biochar. Chem Eng Technol 45:1982–1989. https://doi.org/10.1002/ceat.202200089

Isahak WNRW, Hasan SZ, Ramli ZAC, Ba-Abbad MM, Yarmo MA (2018) Enhanced physical and chemical adsorption of carbon dioxide using bimetallic copper–magnesium oxide/carbon nanocomposite. Res Chem Intermed 44:829–841. https://doi.org/10.1007/s11164-017-3138-6

Ishak N, Nasir AM, Shyang CW, Vo DVN, Hameed BH, Ahmad MA, Din ATM (2024) A review of the current trend in the synthesis of nitrogen-rich functional polymers for carbon dioxide adsorption. Malaysian J Anal Sci 28:461–479. https://www.scopus.com/inward/record.uri?partnerID=HzOxMe3b&scp=85193023314&origin=inward

Karić N, Maia AS, Teodorović A, Atanasova N, Langergraber G, Crini G, Ribeiro ARL, Đolić M (2022) Bio-waste valorisation: Agricultural wastes as biosorbents for removal of (in)organic pollutants in wastewater treatment. Chem Eng J Adv 9:100239. https://doi.org/10.1016/j.ceja.2021.100239

Ke Y, Zhu C, Li J, Liu H, Yuan H (2022) The catalytic oxidation of glycerol over pt supported on mofs-derived carbon nanosheets. ACS Omega 50:46452–46454. https://doi.org/10.1021/acsomega.2c05155

Kongnoo A, Tontisirin S, Worathanakul P, Phalakornkule C (2017) Surface characteristics and CO_2 adsorption capacities of acid-activated zeolite 13X prepared from palm oil mill fly ash. Fuel 193:385–394. https://doi.org/10.1016/j.fuel.2016.12.087

Langmuir I (1918) The adsorption of gases on plane surfaces of glass, mica and platinum. J Am Chem Soc 40:1361–1403. https://doi.org/10.1021/ja02242a004

Lu T, Bai J, Demir M, Hu X, Huang J, Wang L (2022) Synthesis of potassium bitartrate-derived porous carbon via a facile and self-activating strategy for CO_2 adsorption application. Sep Purif Technol 296:121368. https://doi.org/10.1016/j.seppur.2022.121368

The MathWorks, Inc (2024) Decision Tree. MathWorks Official Web. https://ww2.mathworks.cn/help/stats/decision-trees.html. Accessed 15 Nov 2024

The MathWorks, Inc (2024) fitcsvm. MathWorks Official Web. https://ww2.mathworks.cn/help/stats/fitcsvm.html. Accessed 15 Nov 2024

The MathWorks, Inc (2024) Fitctree. https://ww2.mathworks.cn/help/stats/fitctree.html. Accessed 15 November 2024

The MathWorks, Inc (2024) Understanding support vector machine regression. https://ww2.mathworks.cn/help/stats/understanding-support-vector-machine-regression.html?searchHighlight=support vector machine&s_tid=srchtitle_support_results_5_support vector machine. Accessed 15 Nov 2024

Melouki, R, Ouadah, A, Llewellyn, PL (2020) The CO_2 adsorption behavior study on activated carbon synthesized from olive waste. J CO_2 Util 42:101292. https://doi.org/10.1016/j.jcou.2020.101292

MIDA (2023) Equilibrium through carbon capture: Malaysia's path to net-zero emissions. MIDA Official Web. https://www.mida.gov.my/equilibrium-through-carbon-capture-malaysias-path-to-net-zero-emissions/. Accessed 23 Oct 2024

MIDA (2023) Malaysia on track to achieve net zero by 2050. MIDA Official Web. https://www.mida.gov.my/mida-news/malaysia-on-track-to-achieve-net-zero-by-2050/. Accessed 23 Oct 2024

Nandi R, Jha MK, Guchhait SK, Sutradhar D, Yadav S (2023) Impact of KOH activation on rice husk derived porous activated carbon for carbon capture at flue gas alike temperatures with high CO_2/N_2 selectivity. ACS Omega 8:4802–4812. https://doi.org/10.1021/acsomega.2c06955

Nareswari C, Zulfiani U, Junaidi A, Gunawan T, Widiastuti N (2024) Adsorption of CO_2 and H_2 on the polymer-based membrane from high-density

polyethylene (HDPE) plastic. South African J Chem Eng 49:105–113. https://doi.org/10.1016/j.sajce.2024.04.004
Naseer MN, Zaidi AA, Dutta K, Wahab YA, Jaafar J, Nusrat R, Ullah I, Kim B (2022) Past, present and future of materials' applications for CO_2 capture: A bibliometric analysis. Energy Rep 8:4252–4264. https://doi.org/10.1016/j.egyr.2022.02.301
Ogungbenro AE, Quang DV, Al-Ali KA, Vega LF, Abu-Zahra MRM (2020) Synthesis and characterization of activated carbon from biomass date seeds for carbon dioxide adsorption. J Environ Chem Eng 8:104257. https://doi.org/10.1016/j.jece.2020.104257
Pacześniak T, Rydel-Ciszek K, Chmielarz P, Charczuk M, Sobkowiak A (2018) Electrochemical reaction Gibbs energy: Spontaneity in electrochemical cells. J Chem Educ 95:1794–1800. https://doi.org/10.1021/acs.jchemed.7b00871
Pang R, Lu T, Shao J, Wang L, Wu X, Qian X, Hu X (2021) Highly efficient nitrogen-doped porous carbonaceous CO_2 adsorbents derived from biomass. Energy Fuels 35:1620–1628. https://doi.org/10.1021/acs.energyfuels.0c03832
Patel H (2019) Fixed-bed column adsorption study: A comprehensive review. Appl Water Sci 9:1–17. https://doi.org/10.1007/s13201-019-0927-7
Policicchio A, Conte G, Agostino RG, Caputo P, Rossi CO, Godbert N, Nicotera I, Simari C (2022) Hexagonal mesoporous silica for carbon capture: Unrevealing CO_2 microscopic dynamics by Nuclear Magnetic Resonance. J CO_2 Util 55:101809. https://doi.org/10.1016/j.jcou.2021.101809
Puig-Gamero M, Esteban-Arranz A, Sanchez-Silva L, Sanchez P (2021) Obtaining activated biochar from olive stone using a bench scale high-pressure thermobalance. J Environ Chem Eng 9:105374. https://doi.org/10.1016/j.jece.2021.105374
Quan C, Wang H, Jia X, Gao N (2021) Effect of carbonization temperature on CO_2 adsorption behavior of activated coal char. J Energy Inst 97:92–99. https://doi.org/10.1016/j.joei.2021.04.003
Rafique M, Lougou BG, Yong S, Hussain D, Ghorbal A, Wang B (2024) DFT based investigations on inherent CO_2 adsorption and direct dissociation capability of Ti_2C and Nb_2C mxenes. Surfaces and Interfaces 54:105196. https://doi.org/10.1016/j.surfin.2024.105196
Ruthven DM (1984) Principles of adsorption and adsorption processes. Wiley, New York
Sarwar A, Ali M, Khoja AH, Nawar A, Waqas A, Liaquat R, Naqvi SR, Asjid M (2021) Synthesis and characterization of biomass-derived surface-modified activated carbon for enhanced CO_2 adsorption. J CO_2 Util 46:101476. https://doi.org/10.1016/j.jcou.2021.101476
Serafin J, Dziejarski B (2023) Application of isotherms models and error functions in activated carbon CO_2 sorption processes. Microporous Mesoporous Mater 354:112513. https://doi.org/10.1016/j.micromeso.2023.112513
Serafin J, Narkiewicz U, Morawski AW, Wróbel RJ, Michalkiewicz B (2017) Highly microporous activated carbons from biomass for CO_2 capture and effective micropores at different conditions. J CO_2 Util 18:73–79. https://doi.org/10.1016/j.jcou.2017.01.006
Shao J, Ma C, Zhao J, Wang L, Hu X (2022) Effective nitrogen and sulfur co-doped porous carbonaceous CO_2 adsorbents derived from amino acid. Colloids Surfaces A Physicochem Eng Asp 632:127750. https://doi.org/10.1016/j.colsurfa.2021.127750
Shi J, Cui H, Xu J, Yan N (2022) Carbon spheres synthesized from $KHCO_3$ activation of glucose derived hydrochar with excellent CO_2 capture capabilities at both low and high pressures. Sep Purif Technol 294:121193. https://doi.org/10.1016/j.seppur.2022.121193
Siriwardane RV, Shen MS, Fisher EP, Poston JA (2001) Adsorption of CO_2 on molecular sieves and activated carbon. Energy Fuels 15:279–284. https://doi.org/10.1021/ef000241s
Socrates, G (2001) Infrared and Raman characteristic group frequencies. Tables and charts, Journal of Raman Spectroscopy. John Wiley & Sons, England
Sun LB, Kang YH, Shi YQ, Jiang Y, Liu XQ (2015) Highly selective capture of the greenhouse gas CO_2 in polymers. ACS Sustain Chem Eng 3:3077–3085. https://doi.org/10.1021/acssuschemeng.5b00544
Tsiotsias AI, Georgiadis AG, Charisiou ND, Goula MA (2023) CO_2 physisorption over an industrial molecular sieve zeolite: An experimental and theoretical approach. Materials 16:6656. https://doi.org/10.3390/ma16206656
Wang J, Chen S, Xu JY, Liu LC, Zhou JC, Cai JJ (2021) High-surface-area porous carbons produced by the mild KOH activation of a chitosan hydrochar and their CO_2 capture. New Carbon Mater 36:1081–1093. https://doi.org/10.1016/S1872-5805(21)60074-4
Wang S, Lee YR, Won Y, Kim H, Jeong SE, Hwang BW, Cho AR, Kim JY, Park YC, Nam H, Lee DH, Kim H, Jo SH (2022) Development of high-performance adsorbent using KOH-impregnated rice husk-based activated carbon for indoor CO_2 adsorption. Chem Eng J 437:135378. https://doi.org/10.1016/j.cej.2022.135378
Yağmur HK, Kaya İ (2021) Synthesis and characterization of magnetic $ZnCl_2$-activated carbon produced from coconut shell for the adsorption of methylene blue. J Mol Struct 1232:130071. https://doi.org/10.1016/j.molstruc.2021.130071
Zainudin NF, Lee KT, Kamaruddin AH, Bhatia S, Mohamed AR (2005) Study of adsorbent prepared from oil palm ash (OPA) for flue gas desulfurization. Sep Purif Technol 45:50–60. https://doi.org/10.1016/j.seppur.2005.02.008
Zhang Z, Xu M, Wang H, Li Z (2010) Enhancement of CO_2 adsorption on high surface area activated carbon modified by N_2, H_2 and ammonia. Chem Eng J 160:571–577. https://doi.org/10.1016/j.cej.2010.03.070
Zhang J, Zhang X, Li X, Song Z, Shao J, Zhang S, Yang H, Chen H (2024) Prediction of CO_2 adsorption of biochar under KOH activation via machine learning. Carbon Capture Sci Technol 13:100309. https://doi.org/10.1016/j.ccst.2024.100309
Zhou H, Rayer C, Antonangelo AR, Hawkins N, Carta M (2022) Adjustable functionalization of hyper-cross-linked polymers of intrinsic microporosity for enhanced CO_2 adsorption and selectivity over N_2 and CH_4. ACS Appl Mater Interfaces 14:20997–21006. https://doi.org/10.1021/acsami.2c02604

Publisher's Note